



This is a repository copy of *Rotation plays a role in the generation of magnetic fields in single white dwarfs*.

White Rose Research Online URL for this paper:

<https://eprints.whiterose.ac.uk/209295/>

Version: Published Version

Article:

Hernandez, M.S. orcid.org/0000-0001-5103-2713, Schreiber, M.R. orcid.org/0000-0003-3903-8009, Landstreet, J.D. orcid.org/0000-0001-8218-8542 et al. (5 more authors) (2024) Rotation plays a role in the generation of magnetic fields in single white dwarfs. *Monthly Notices of the Royal Astronomical Society*, 528 (4). pp. 6056-6074. ISSN 0035-8711

<https://doi.org/10.1093/mnras/stae307>

Reuse

This article is distributed under the terms of the Creative Commons Attribution (CC BY) licence. This licence allows you to distribute, remix, tweak, and build upon the work, even commercially, as long as you credit the authors for the original work. More information and the full terms of the licence here:

<https://creativecommons.org/licenses/>

Takedown

If you consider content in White Rose Research Online to be in breach of UK law, please notify us by emailing eprints@whiterose.ac.uk including the URL of the record and the reason for the withdrawal request.



eprints@whiterose.ac.uk
<https://eprints.whiterose.ac.uk/>

Rotation plays a role in the generation of magnetic fields in single white dwarfs

Mercedes S. Hernandez ^{1,2}★ Matthias R. Schreiber ^{1,2}★ John D. Landstreet ^{3,4} Stefano Bagnulo ³,
Steven G. Parsons ⁵, Martin Chavarria,^{1,2} Odette Toloza ^{1,2} and Keaton J. Bell ⁶

¹Departamento de Física, Universidad Técnica Federico Santa María, Av. España 1680, Valparaíso, Chile

²Millennium Nucleus for Planet Formation, NPF, Valparaíso 2340000, Chile

³Armagh Observatory and Planetarium, College Hill, Armagh BT61 9DG, Northern Ireland, UK

⁴Department of Physics and Astronomy, University of Western Ontario, London, ON N6A 3K7, Canada

⁵Department of Physics and Astronomy, University of Sheffield, Sheffield S3 7RH, UK

⁶Department of Physics, Queens College, City University of New York, Flushing, NY-11367, USA

Accepted 2024 January 26. Received 2024 January 23; in original form 2023 May 24

ABSTRACT

Recent surveys of close white dwarf binaries as well as single white dwarfs have provided evidence for the late appearance of magnetic fields in white dwarfs, and a possible generation mechanism, a crystallization and rotation-driven dynamo has been suggested. A key prediction of this dynamo is that magnetic white dwarfs rotate, at least on average, faster than their non-magnetic counterparts and/or that the magnetic field strength increases with rotation. Here we present rotation periods of ten white dwarfs within 40 pc measured using photometric variations. Eight of the light curves come from *TESS* observations and are thus not biased towards short periods, in contrast to most period estimates that have been reported previously in the literature. These *TESS* spin periods are indeed systematically shorter than those of non-magnetic white dwarfs. This means that the crystallization and rotation-driven dynamo could be responsible for a fraction of the magnetic fields in white dwarfs. However, the full sample of magnetic white dwarfs also contains slowly rotating strongly magnetic white dwarfs which indicates that another mechanism that leads to the late appearance of magnetic white dwarfs might be at work, either in addition to or instead of the dynamo. The fast-spinning and massive magnetic white dwarfs that appear in the literature form a small fraction of magnetic white dwarfs, and probably result from a channel related to white dwarf mergers.

Key words: magnetic fields – stars: rotation – starspots – white dwarfs.

1 INTRODUCTION

White dwarfs have been speculated to have strong (> 1 MG) magnetic fields many decades ago when Blackett (1947) postulated that the presumed fast rotation of white dwarfs can drive a dynamo, but the first detection of a magnetic white dwarf was obtained more than twenty years later (Kemp et al. 1970). Ever since this groundbreaking discovery, the question of why some white dwarfs become strongly magnetic, while others do not, represents an unsolved questions of stellar evolution.

Today we know large numbers of magnetic white dwarfs. One of the most puzzling facts is the different fractions of strongly magnetic white dwarfs among single stars and in different binary star settings. The volume-limited sample of magnetic single white dwarfs established by Bagnulo & Landstreet (2021) shows that the fraction of magnetic white dwarfs increases with age and is about 20 per cent. Studies of the (incomplete) local 40 pc sample of white dwarfs shows that massive white dwarfs (which are absent in the

20 pc sample) often exhibit strong magnetic fields during the initial stages of the cooling phase (Bagnulo & Landstreet 2022).

A high incidence of magnetic white dwarfs, i.e. around 36 per cent, is seen among cataclysmic variables (CVs), semi-detached close binary stars in which a white dwarf accretes from a Roche-lobe filling main sequence star (Pala et al. 2020).

Intriguingly, among the progenitors of CVs, detached white dwarf plus main-sequence star binaries, the fraction of systems with strongly magnetic white dwarfs is negligible (Liebert et al. 2005, 2015). Of the more than one thousand known systems (Schreiber et al. 2010; Rebassa-Mansergas et al. 2016), only about a dozen magnetic white dwarfs have been serendipitously identified (e.g. Reimers, Hagen & Hopp 1999). In these few detached magnetic white dwarf binaries, the main sequence star companions are close to Roche-lobe filling and the white dwarfs have effective temperatures below 10 000 K (Parsons et al. 2021). The only exception to this trend is the weakly magnetic white dwarf in the young post common envelope binary CC Cet (Wilson et al. 2021). In the majority of the cold detached and strongly magnetic white dwarf binaries, the white dwarf rotation is synchronized with the orbital motion of the secondary star. The only clear exceptions are AR Sco, the first radio-pulsing white dwarf binary star (Marsh et al. 2016), its recently discovered analogue, J191213.72–441045.1 (Pelisoli et al. 2023),

* E-mail: mercedes.hernandez@usm.cl (SSH); matthias.schreiber@usm.cl (MRS)

and 2MASS J0129+6715 which also shows some indications for non-synchronous rotation (Hakala et al. 2022).

Different again is the situation in close double white dwarfs. These systems must have evolved through two phases of mass transfer. Among the dozens of known detached close double white dwarf binaries, only one strongly magnetic white dwarf is known (Kawka et al. 2017; Schreiber et al. 2022). This may indicate that the fraction of systems with magnetic fields may be rather low or that detecting magnetic fields in double white dwarfs can be extremely challenging. Only very recently, the first potentially weakly magnetic white dwarfs have been detected among semi-detached double white dwarfs, the so-called AM CVn binaries (Maccarone et al. 2024).

Several ideas have been put forward to explain the origin of strongly magnetic white dwarfs. The three most popular scenarios that have been suggested in the last decades are (i) the fossil field scenario in which the magnetic field of the progenitor of the white dwarf is preserved during the white dwarf formation (e.g. Angel, Borra & Landstreet 1981; Braithwaite & Spruit 2004; Wickramasinghe & Ferrario 2005); (ii) a dynamo generated during common-envelope evolution in close binaries (Regós & Tout 1995; Tout et al. 2008; Wickramasinghe, Tout & Ferrario 2014), and (iii) coalescing double degenerate cores/objects (García-Berro et al. 2012). However, all three scenarios face serious difficulties when compared to observations. The relative numbers of strongly magnetic white dwarfs predicted by the fossil field scenario are far lower than the observed numbers if updated star formation rates and evolutionary time-scales are taken into account (Kawka & Vennes 2004). The solution to this problem suggested by Wickramasinghe & Ferrario (2005), who postulated the existence of a large number of main sequence stars slightly less magnetic than Ap and Bp stars, was refuted by spectropolarimetric surveys (Aurière et al. 2007).

The common envelope dynamo scenario in its current form predicts relative numbers of magnetic systems far too large when compared to observations (Belloni & Schreiber 2020), and the biggest weakness of the double degenerate merger scenario is that it cannot explain a large number of magnetic white dwarfs among CVs. In addition, all three scenarios do not offer an explanation for the absence of young detached magnetic white dwarf binaries (e.g. Liebert et al. 2005) and the late appearance of the magnetic fields in single white dwarfs (Bagnulo & Landstreet 2021).

Based on the idea originally put forward by Isern et al. (2017), an alternative model to explain the incidence of magnetic fields in white dwarfs has been recently suggested by Schreiber et al. (2021a). This scenario has been shown to explain a large number of observations of magnetic white dwarfs in binaries: the increased occurrence rate of magnetic white dwarfs in CVs, the paucity of magnetic white dwarfs in the sample of observed double white dwarfs, the relatively large number of detached but close to Roche-lobe filling cold magnetic white dwarf plus M-dwarf binaries, the existence of radio-pulsating white dwarfs such as AR Sco (Schreiber et al. 2021a, b, 2022), as well as the absence of high accretion rate polars in globular clusters (Belloni et al. 2021). One of the key predictions originally made by this scenario is that strongly magnetic crystallizing white dwarfs should rotate significantly faster than non-magnetic white dwarfs.

However, Ginzburg et al. (2022) recently suggested that the convective turnover times in crystallizing white dwarfs are orders of magnitude longer than previously thought. If this is true, white dwarfs with spin periods of several hours or even days can generate magnetic fields of the order of an MG. If super-equipartition is assumed (Augustson et al. 2016), even much stronger fields, such as those observed in many CVs, covering the range of 1–100 MG can be produced. Crucial for the context of this paper, this model predicts a

relation between spin period and field strength. However, testing this hypothesis, i.e. faster rotation in magnetic than non-magnetic white dwarfs and/or a relation between field strength and rotation requires a representative sample of spin periods of magnetic white dwarfs.

Magnetic white dwarfs can show photometric variability which allows for measuring their spin periods. This variability can have different origins. In convective atmospheres starspots can be generated by the magnetic field. As these regions are cooler and darker, starspots rotating into view, reduce the observed brightness. A strong magnetic field might however completely inhibit convection in the atmospheres, which makes the appearance of starspots unlikely (Tremblay et al. 2015). Alternatively, the Balmer lines can be split and shifted to the blue due to the presence of a strong magnetic field. The amount of this shift depends on the local field strength, which will change the spectral energy distribution locally (even if the flux remains unchanged), leading to light variation in observations in a single passband if the local field strength varies much over the stellar surface. This effect would predict larger variations (on average) in stars with stronger fields, and maybe larger amplitudes in hotter white dwarfs with stronger Balmer line blocking (Hardy, Dufour & Jordan 2023). A third potential origin of photometric variability is that the polarized line opacities depend on the local field strength and on the angle a given region is looked at. The latter is probably a smaller effect, but might account for variations of the order of one percent in some cases. Finally, magnetic fields can cause metals to be distributed non-homogeneously on the white dwarf surface which can cause photometric variations as well (Dupuis et al. 2000). Independent of the exact mechanism producing the variability, photometric variability of magnetic white dwarfs allows for measuring their rotation rates.

The volume-limited sample of white dwarfs within 20 pc contains 33 magnetic white dwarfs (Bagnulo & Landstreet 2021). This sample is ideal to study by measuring the rotation periods of a representative sample of magnetic white dwarfs thereby potentially constraining scenarios for the origin of magnetic fields. We found that 27 of these magnetic white dwarfs have been observed with *TESS* (*Transiting Exoplanet Survey Satellite*; Ricker et al. 2015). The resulting light curves show statistically significant and constant periodic signals (the same period in all *TESS* sectors) in only five cases. Given this small sample size, we included all known magnetic white dwarfs within 40 pc and identified three more periods. In addition to analysing the *TESS* light curves, we followed up two additional targets (one of them part of the 20 pc sample) with SPECULOOS (Search for habitable Planets Eclipsing ULtra-cOOl Star; Delrez et al. 2018; Jehin et al. 2018). We compared our period measurements to those non-magnetic and magnetic white dwarfs with previously measured spin periods, and finally, we discuss possible implications for the origin of magnetic fields in white dwarfs.

2 OBSERVATIONS

In this work, we combine photometric data of magnetic white dwarfs from *TESS* with light curves obtained using the SPECULOOS instrument. In what follows we briefly describe the data acquisition for both cases as well as the procedure we used for determining the rotational period.

2.1 *TESS*

For all magnetic white dwarfs within 20 pc listed in Bagnulo & Landstreet (2021) we searched for *TESS* light curves. Of the 33 targets on the list, we found *TESS* observations for 27 magnetic

white dwarfs which are listed in Table A1 with their corresponding sectors. We also took a careful look at the new magnetic white dwarfs identified in the 40 pc sample (Bagnulo & Landstreet 2022; O’Brien et al. 2023) *TESS* data are available for 23 of the 30 new magnetic white dwarfs (O’Brien et al. 2023; their table A1) and for eight white dwarfs from Bagnulo & Landstreet (2022), all listed in Table A2.

The *TESS* light curves were obtained from the Mikulski Archive for Space Telescopes (MAST¹) web service. We extracted the Pre-search Data Conditioned Simple Aperture Photometry (PDCSAP) which removes trends caused by the spacecraft, and removed all data points with a non-zero quality flag and all NaN values in each sector.

Contaminating flux from unexpected sources which occurs due to a combination of pixel size and flux integration is a known issue in *TESS* light curves. We therefore performed a test to identify possible contaminating flux in the light curves using the flux contamination tool² (FLUXCT; Schonhut-Stasik & Stassun 2023). We note that this tool is based on *Gaia* G-band magnitudes of the objects in each pixel, i.e. the tool is using a band-pass different from *TESS*. Therefore, the estimated levels of contamination may not be entirely accurate. How much the real values deviate from the estimates depends on the colours of the source and contaminants. However, given that the two bands overlap, our estimates should not differ from the real contamination level by more than a few per cent in most cases.

We emphasize that a critical examination of the data of each target is fundamental to avoid wrong conclusions being drawn. To that end, we slightly modified the code that provides contamination levels for *TESS* targets. The original version only offers the contamination level and the *Gaia* G-magnitude of the target for the first observed sector. More insight can be gained by providing the contamination level and G-magnitude of the target for each sector.

We analysed each sector of each target with the least-squares spectral method based on the classical Lomb–Scargle periodogram (Lomb 1976; Scargle 1982) to obtain the main period of the photometric *TESS* data. For each star, we started with the least contaminated sector to make sure the signal we are picking up is coming from the white dwarf and then requested the detected period to show up with a consistent amplitude in all other sectors. We searched for periods in frequency space up to the Nyquist frequency.

To make sure the signal is significant, we also performed a false alarm probability (FAP) test. We formally requested this FAP to be below 5 per cent. For all the periods we detected we found the FAP to be less than 10^{-6} . The uncertainties of the periods were computed using the curfit routine from Bevington (1969), which is a Levenberg–Marquardt non-linear least-squares fitting procedure.

In case a given white dwarf light curve passed all the above tests we finally inspected adjacent *TESS* pixels to check whether nearby bright stars could have contaminated the white dwarf light curve. The FLUXCT mentioned above only provides information on stars located within the same *TESS* pixel. We therefore used the LIGHTKURVE tool (Lightkurve Collaboration 2018) for this exercise. If a bright source was found we downloaded its *TESS* light curve (in case available) and ran a period search. If the same period was found as for the white dwarf, we used the amplitude of the variation to decide if the photometric variability is indeed coming from the white dwarf.

As a first example that illustrates the importance of a careful analysis of *TESS* data, we show in the appendix (Fig. A1) the light curve we obtained for WD 2150+591. A very strong signal is clearly present in the data with a period of 116.38 h. However, the amplitude

largely exceeds those found for other white dwarfs and the light curve resembles that of an eclipsing binary. The up-dated FLUXCT provided the G-magnitude for the target of each sector which revealed that the G-magnitude of the target in the first sector was clearly different to that of WD 2150+591. In other words, the detected star in the first sector was a nearby eclipsing binary instead of the white dwarf we aimed to analyse, and we therefore eliminated this white dwarf from our sample of systems with measured period.

Taking a detailed look at adjacent pixels with the LIGHTKURVE TOOL turned out to be important as well. In one case (WD 1009-184), we indeed found that the period measured from the white dwarf light curve most likely corresponds to that of a nearby bright star (Fig. 1) and we excluded the white dwarf from our sample of stars with reliable periods. Bagnulo & Landstreet (2019) report variations on the magnetic field strength based on two measurements for this white dwarf but more measurements are needed to constrain the spin period.

Up to this point, we have identified a total of 18 white dwarfs exhibiting significant variability: 11 within 20 pc and 7 within 40 pc. For a final decisive test, we analysed all 18 white dwarfs with the new tool TESS_LOCALIZE³ (Higgins & Bell 2023). This tool is especially designed to localize the source most likely responsible for observed variations in each *TESS* pixel. TESS_LOCALIZE delivers the optimized column and row coordinates corresponding to the most probable location of the observed variability. The algorithm complements *TESS* using queries to the *Gaia* Archive⁴ (Gaia Collaboration 2021) for star locations and offers metrics such as *p*-values and relative likelihoods to facilitate interpretation of the fit outcomes. Prior to the fitting process, the TESS_LOCALIZE tool offers the option to discern prevalent trends among pixels located outside the designated aperture. This task is accomplished through principal component analysis (PCA). The resulting PCA components can be effectively applied to and subtracted from the light curves extracted by TESS_LOCALIZE. None the less, it is imperative to ensure that these PCA trends do not represent the signals targeted for localization; otherwise, the signals may be inadvertently removed from the data. It is important to note that TESS_LOCALIZE should provide a substantial detection, meaning that the ‘height’ parameter in the fit is significantly different from zero given its uncertainty, ensuring it is not a false positive detection.

Eighteen targets were initially considered but 10 were subsequently eliminated from the sample due to TESS_LOCALIZE results showing that the signals observed in the light curves did not originate from the white dwarf targets. These eliminated targets are as follows: WD 0810-353, WD 0816-310, WD 1036-204, WD 1829-547, WD 1900+705, and WD 2153-512 from the 20 pc sample and WD 0232+525, WD 1008-242, WD J091808.59-443724.25, and WD J094240.23-463717.68 from the 40 pc sample. For all the white dwarfs discarded with TESS_LOCALIZE, the origin of the detected variation was well located on the field with the exception of WD 1008-242 where we were unable to identify the source of the measured variability.

Considering all tests listed above, the final sample of white dwarf periods measured from *TESS* contains eight white dwarfs, five with distance less than 20 pc and three within the 40 pc. For these systems the average G-magnitude in the *TESS* sectors is in agreement with the one reported in literature for the corresponding white dwarf and contamination from nearby sources can be excluded as the source of the identified variations. The contamination level and the exposure

¹<https://mast.stsci.edu>

²<https://www.jessicastasik.com/flux-contamination-tool>

³github.com/Higgins00/TESS-Localize

⁴<https://gea.esac.esa.int/archive/>

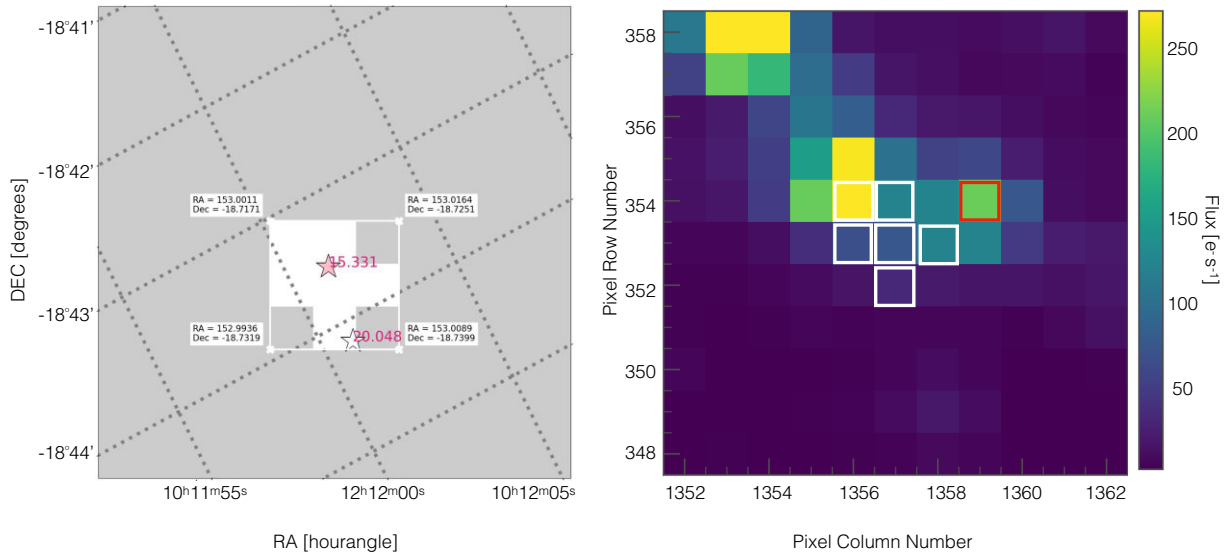


Figure 1. The pixel view obtained with the two different tools used to study the contamination from nearby sources to the white dwarf observed with *TESS*. Left: The FLUXCT provides a white area corresponding to the pixels used to calculate the contamination. The position of WD 1009-184 is indicated by a pink star while that of the only contaminating source found by the tool is shown as a white star. The numbers right next to each star indicate their *Gaia* G-magnitudes. Right: The image obtained with the LIGHTKURVE TOOL. Pixels with a white edge were used to extract the *TESS* light curve of WD 1009-184. The variation found in the light curve of this system, however, results from contamination of these pixels from a bright star in the pixel with the red border. The star located in this pixel shows cleaner variations with the same period and a larger amplitude. This type of contamination cannot be identified if *TESS* data are only analysed with the FLUXCT. However, TESS_LOCALIZE confirms that the origin of the variation corresponds to target Gaia DR3 5669427508702256896 located at the pixel marked with the red border.

times of each *TESS* sector of the confirmed white dwarfs are shown in Tables A1 and A2. The measured periods, G magnitudes and normalized amplitudes obtained from *TESS* light curves as well as the frequencies and PCA entries for the TESS_LOCALIZE tool and the best fits results (p -values and likelihood) for the eight targets with clear, significant, and consistent variations (that can be assumed to reflect the rotation period) are listed in Table 1. The periodograms and the phase-folded light curves (which include all the sectors mentioned in Tables A1 and A2) for each of the eight *TESS* targets are shown in Fig. 2.

The periodicity in the light curves of WD 0009+501, WD 0011-134, WD 0011-721, WD J075328.47–511436.98, and WD J171652.09–590636.29 is difficult/impossible to spot in the phase folded light curves. With the aim to provide a better visualization of the five mentioned light curves, we therefore calculated the mean flux for 100 bins. The corresponding folded light curves are shown in Fig. 2. As mentioned earlier, the FAP for the highest peak in each periodogram is below 10^{-6} . We illustrate the FAP level corresponding to a probability of 10^{-3} in all periodograms in Fig. 2. We note that in two cases, WD 0009+501 and WD 0041-102, a second highly significant peak appears in the periodograms. Previous observations show that these two highest peaks correspond to the rotation period of these two white dwarfs (Achilleos et al. 1992; Valyavin et al. 2005a). The light curves folded over the true rotation period are shown in Fig. A2 in the appendix.

2.2 SPECULOOS

For two white dwarfs, WD 2138-332 (part of the 20 pc sample) and LSPMJ0107+2650 (a more distant magnetic DZ white dwarf), we performed observations with the SPECULOOS Southern Observatory (SSO). SPECULOOS is composed of four telescopes with primary mirrors of 1.0 m diameter, run by the European Southern

Observatory (ESO) and located at Paranal, Chile. We used the SPECULOOS/Y4KCam CCD with the *SDSS* g' filter. This filter covers the range where the Balmer lines β and γ , and some of the strongest Helium lines, can be found when observing white dwarfs. The dates, exposure times, and the name of the telescope that was used are listed in Table B1.

Data reduction was performed using PROSE (Garcia et al. 2022), a Python framework to build a modular and maintainable image processing pipeline. Dark, bias, and flat field corrections were executed to all the images, followed by an automated line-up in preparation for the aperture photometry. We then analysed the resulting photometry with the least-squares spectral method used for *TESS* targets and found that both targets showed clear variation associated with the rotation of the white dwarf. For WD 2138-332, the periodogram shows several aliases, and the light-curve fit is reasonable with a number of different periods between 4 and 12 h, with 6.19 h corresponding to the highest peak in the periodogram providing the best fit. However, with the data currently available, we can only constrain the period to be between 4 and 12 h. Spectral type, effective temperature, mass and magnetic field strengths (Hollands et al. 2017; Bagnulo & Landstreet 2019) together with the rotational period measured with SPECULOOS are listed in Table 1, while the periodograms and the phase-folded light curves are shown in Fig. 3.

3 THE ROTATION PERIODS OF MAGNETIC WHITE DWARFS

We have measured periodic photometric variations for ten magnetic white dwarfs, five of which are within a distance of 20 pc. In addition, eight of these periods have been obtained from *TESS* light curves which cover at least one month of continuous observations and are therefore not biased towards short periods, in contrast to those determined from short (a few days) observing runs using ground-

Table 1. Rotation periods measured from *TESS* and *SPECULOOS* together with their normalized amplitudes. We provide two period approximations for WD 2138-332, i.e. the period corresponding to highest peak in the periodogram which represents the best fit and the range of possible rotational periods given the data currently available. The extra line for WD 0009+501 and WD 0041-102 provides the rotational period measured through independent observations by Bagnulo, Landstreet & Valyavin (in preparation) and Achilleos et al. (1992) which correspond to twice the period measured with *TESS* (see Section A3 for more details). We provide the entries for the *TESS_LOCALIZE* tool; TIC name, the frequency measured from the *TESS* light curves, and the number of signals removed (PCA) to obtain the best signal to noise for the signal fitting. Finally, we present the resulting *p*-values and relative likelihoods for the best-fitting indicating that the white dwarf is the variable source.

Name	TIC name	<i>Gaia</i> DR3	G (mag)	Period (h)	Frequency (μ Hz)	PCA	<i>p</i> -value	Likelihood (per cent)	Normalize amplitude
<i>TESS</i>									
WD 0009+501	TIC 201892746	395 234 439 752 169 344	14.23	4.0086 \pm 0.0001	69.2954592071	3	0.597	0.99	0.0034 \pm 0.0003
				8.016 \pm 0.083	34.69620007	0	0.038	0.99	0.0042 \pm 0.0002
WD 0011-134	TIC 289712694	2 418 116 963 320 446 720	15.75	0.736 \pm 0.007	377.415458937	0	0.536	1.0	0.0033 \pm 0.0004
WD 0011-721	TIC 328029653	4 689 789 625 044 431 616	15.03	14.13 \pm 0.38	19.6566378500	0	0.127	0.99	0.0038 \pm 0.0003
WD 0912+536	TIC 251080865	1 022 780 838 739 029 120	13.78	31.93 \pm 0.13	8.69795145847	0	0.667	1.0	0.0189 \pm 0.0001
WD 2359-434	TIC 321979116	4 994 877 094 997 259 264	12.89	2.694 \pm 0.002	103.109791305	0	0.413	1.0	0.0037 \pm 0.0001
WD 0041-102	TIC 3888273	2 377 863 773 908 424 448	14.5	1.0967 \pm 0.0007	253.44687753	0	0.542	1.0	0.0290 \pm 0.0003
				2.19 \pm 1.09	126.723438767	0	0.379	1.0	0.0327 \pm 0.0003
WD J075328.47-511436.98	TIC 269071459	5 513 896 164 414 899 456	15.6	21.51 \pm 0.01	12.9084891387	2	0.369	1.0	0.0062 \pm 0.0005
WD J171652.09-590636.29	TIC 380174982	5 915 797 694 789 556 096	15.62	4.4398 \pm 0.0003	62.5653808229	0	0.297	0.96	0.0080 \pm 0.0001
<i>SPECULOOS</i>									
LSPM J0107+2650	-	306 779 618 349 361 920	18.88	4.83 \pm 0.29	-	-	-	-	0.11 \pm 0.01
WD 2138-332	TIC 204440456	6 592 315 723 192 176 896	14.44	6.19 \pm 0.05 4.0-12.0	-	-	-	-	0.008 \pm 0.001

based telescopes. In what follows we compare our findings with periods of magnetic and non-magnetic white dwarfs provided in the literature.

Most rotation periods of magnetic white dwarfs result from photometric measurements with ground-based telescopes such as the two periods we determined with *SPECULOOS*. Additional periods have been determined through variations in the polarization degree. Given the fact that it is virtually impossible to use ground-based telescopes to reach the same cadence and baseline as the *Kepler* surveys or *TESS*, the full sample of rotation periods of magnetic white dwarfs is likely biased towards shorter periods when compared to that of non-magnetic white dwarfs.

We used two different approaches towards a more representative samples of magnetic white dwarf spin periods. First, we only used periods measured from *TESS* light curves, except for WD 0009+501, whose period measured with *TESS* is half of the real period measured with spectropolarimetry. The cadence and baseline of *TESS* is much longer than the periods measured for non-magnetic white dwarfs. Therefore, the eight periods we measured from *TESS* (Table 1) should not be biased towards shorter periods, and thanks to the very short exposure time in some of the sectors (20 s), the chances to miss an extremely short spin period are low. The obvious disadvantage of this sample is its small size.

Because of the small size of the *TESS* sample, we also establish a volume-limited sample consisting of spin periods of magnetic white dwarfs within 20 pc. This sample combines five period measurements from *TESS*, the rough period estimate we obtained for WD 2138-332, and four periods of magnetic white dwarfs within 20 pc from the literature (Table C1). This results in a sample of ten magnetic white dwarfs with measured rotation period within 20 pc which represents 30 per cent of the 20 pc sample of magnetic white dwarfs. The disadvantage of this sample is that it is incomplete and might again be biased towards short periods.

3.1 Comparison with previously identified periods of magnetic white dwarfs

To compare our results with previously measured rotation periods of magnetic white dwarfs, we established a list of robustly measured rotational periods from the literature, i.e. in what follows we ignore uncertain period estimates or measurements that provided a range of possible periods. Our final sample of magnetic white dwarfs with robustly measured periods from the literature is given in Table C1. It contains seven white dwarfs from Brinkworth et al. (2013), who presented observations of 30 isolated magnetic white dwarfs performed with the Jacobus Kapteyn Telescope and compiled a list of previously published periods. We further complemented our literature search by going through the periods listed in Kawka et al. (2007) and Ferrario, de Martino & Gänsicke (2015) – ignoring rather rough estimates – and by adding more recent measurements. In addition, we list three yet unpublished periods measured by Landstreet and Bagnulo through polarimetry. The observations that allowed the determination of these periods will be published elsewhere. This compilation of literature encompasses a total of 42 white dwarfs with reliably measured spin periods. Five of these 42 are in our *TESS* sample. Six of these 42 magnetic white dwarfs are very likely the product of the merger of two degenerate stars, as they are very massive white dwarfs ($> 1.25 M_{\odot}$) with rotation periods below 0.38 h. An atypical result of a merger is SDSS J125230.93-023417.72 with low mass ($0.58 M_{\odot}$; Reding et al. 2023). Occasionally we eliminate these likely merger products from the sample in order to constrain

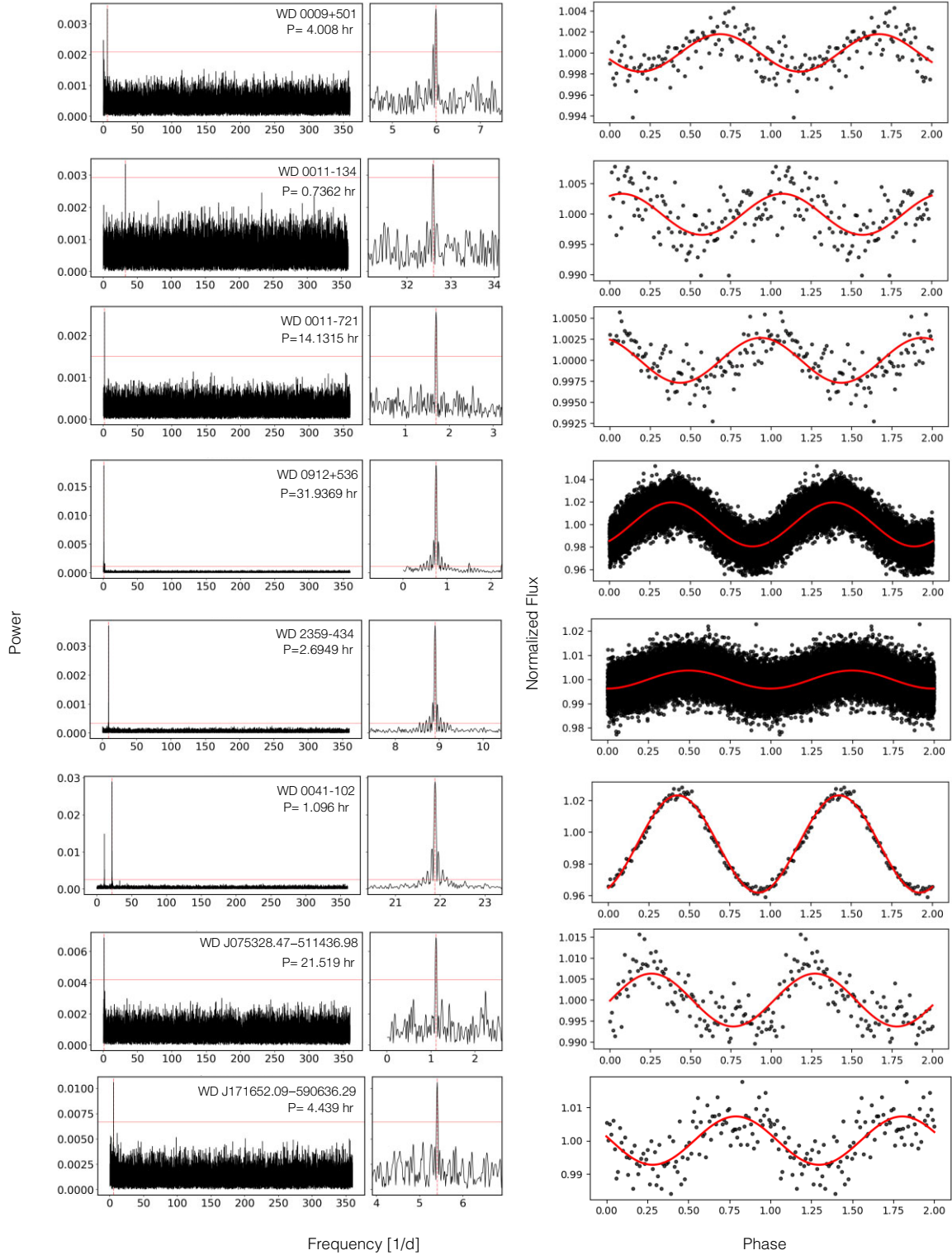


Figure 2. Periodograms (left: full Nyquist range; middle: zoomed in to the highest peak) and phase-folded light curves (right) of eight white dwarfs with a *TESS* light curve that shows statistically significant variations with the same period in all available sectors. The horizontal red line illustrates the false alarm probability level (FAP level) for a probability of 10^{-3} per cent. In the case of WD 0009+501, WD 0011-134, WD 0011-721, WD 0041-102, WD J075328.47-511436.96, and WD J171652.09-590636.29 we binned the phase-folded light curve (using 100 bins) as the amplitude of the variation is too small to be spotted in the un-binned light curve. For WD 0009+501 and WD 0041-102 we know from previous observations that the true period is twice the period we detect in the *TESS* data (Achilleos et al. 1992; Valyavin et al. 2005). We use the longer (and correct) periods in the distributions discussed in this paper. The *TESS* light curves folded over the rotation period can be found in the appendix. For the other seven objects, we interpret the observed periods as reflecting the rotation periods of the white dwarfs. The measured periods range from a few hours to several days.

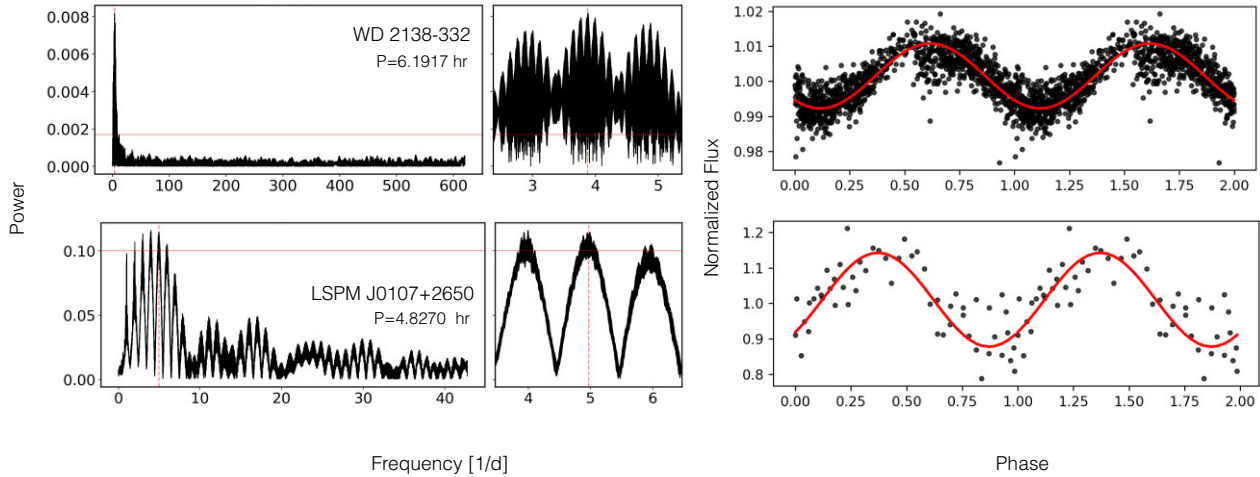


Figure 3. Periodograms (left: full Nyquist range; middle: zoomed in to the highest peak) and phase-folded light curves (right) of the two white dwarfs observed with SPECULOOS. The obtained periods are less certain than those measured from *TESS* light curves. The horizontal red line illustrates the false alarm probability level (FAP level) for a probability of 10^{-6} per cent. For WD 2138-332 we can estimate only a range of periods because several periods (peaks in the periodogram) provide reasonable fits to the data. However, both targets clearly have periods of the order of a few hours.

other possible mechanisms for generating the white dwarf magnetic fields.

We start the comparison of our samples with previously published spin periods with WD 0912+536. This white dwarf was one of the first known magnetic white dwarfs and was found to show periodic variations in circularly polarized light with a period of ≈ 32.16 h (Angel & Landstreet 1971). The most obvious explanation for periodic variations in polarized light is the rotation of the white dwarf in combination with a magnetic field that is not symmetrical about the spin axis. The period we determined from the *TESS* light curve (31.93 h) is very close to the value measured by Angel & Landstreet (1971). This agreement confirms that we can indeed assume periodic light-curve variations to reflect the rotational periods. Other examples for spin periods measured with *TESS* and through polarimetry are WD 0011-134 and WD 2359-434, in both cases the periods also agree (compare Table 1 with Table C1). An interesting example is WD 0009+501. For this star Valyavin et al. (2005) finds the magnetic field to be variable with a period of eight hours and Valeev et al. (2015) found photometric variability confirming this period but mentioned that the light curve showed two maxima per period. The *TESS* light curve confirms this finding but without the knowledge of the field strength variability, we would have interpreted the stronger periodic signal as the rotation period (4 h) which is in fact half the real rotation period. The *TESS* light curve folded over the true rotation period is shown in Fig. A2 in the appendix.

Also the highest peak in the periodogram of WD 0041-102 corresponds to half the rotational period previously measured. If we fold the light curve over the period derived by Achilleos et al. (1992), we find two humps of different amplitudes in agreement with their results (see Fig. A2 in the appendix). Achilleos et al. (1992) showed that this variation is produced by a magnetic field that is dipolar and orientated at about 90 degrees to the spin axis. Thus, as the star spins, the abundance pattern on the surface seen from Earth varies. The strength of spectral lines, the flux they block directly, and the line blocking bluewards of the Balmer jump, as seen from Earth, also change as the star rotates. This most likely produces the very strong light variability of this star. For an alternative interpretation for white dwarfs displaying two minima in their light curves see Farihi et al. (2023).

It is worth pointing out that a similar issue as identified for WD 0009+501 and WD 0041-102 could affect virtually all our other targets (i.e. we could be off by a factor of 2 for most objects). However, even if this is the case the conclusions presented in this paper would not change.

To evaluate whether the *TESS* and the 20 pc samples we defined are systematically different to the periods of magnetic white dwarfs in the literature we performed a Kolmogorov–Smirnov (KS) test and show the cumulative distributions in Fig. 4. Assuming the usual 2-sigma significance criterion (p -values below 0.05) to reject the Null-hypothesis (both distributions come from the same parent distribution), both our samples do not show significant indications for being different to that of magnetic white dwarfs we found in the literature (Table 2). More precisely, the observed differences have an unacceptable high probability to be caused by chance (exceeding 30 per cent). We also compare the average and median values of our samples and those of previously identified periods of magnetic white dwarfs and find comparable values (Table 2). For this exercise, we also excluded magnetic white dwarfs that are very likely the product of a merger (very fast-spinning, i.e. $P < 0.38$ h and very massive, i.e. $M > 1.25 M_{\odot}$, white dwarfs) in agreement with the predictions made by Schwab (2021). These white dwarfs are WD 0316-849, WD 1859+148, WD 2254+076, WD 2209+113, Gaia DR3 4479342339285057408, and ZTF J1901+1458. While the median values in our samples are slightly longer than those of previously identified periods (even if we exclude mergers), the average periods are somewhat shorter. We conclude that the more representative samples defined here do not show significant differences to previously measured periods of magnetic white dwarfs.

3.2 Comparison with non-magnetic white dwarfs

Hermes et al. (2017a) and Kawaler (2015) used data from the *Kepler* space telescope to measure the spin periods of pulsating non-magnetic white dwarfs and found that the mean spin period of isolated non-magnetic white dwarfs with masses in the range of $0.51 - 0.72 M_{\odot}$ is ≈ 35 h with a standard deviation of 28 h. In other words, the majority of non-magnetic white dwarfs have spin periods between 0.5 and 3 d. In the context of the crystallization and rotation-

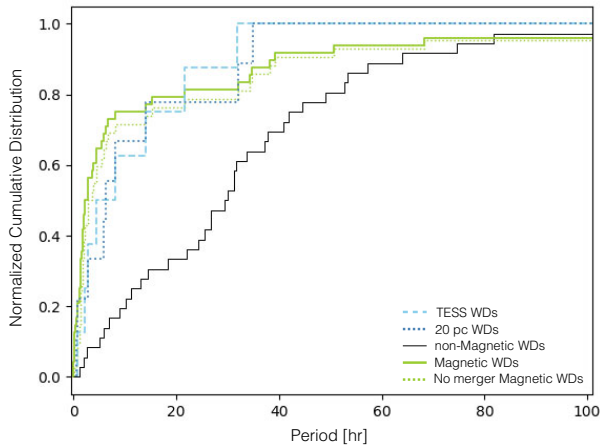


Figure 4. Cumulative period distributions of magnetic and non-magnetic white dwarfs. If we consider all rotation periods measured for magnetic white dwarfs (solid green line) and the magnetic white dwarf after removing white dwarfs that most likely result from mergers (dotted green line), they seem to rotate significantly faster than non-magnetic white dwarfs (solid black line). A KS-test between the full magnetic and non-magnetic sample gives a probability of only 3.76×10^{-7} for the observed difference to be caused by chance. However, this is clearly caused by an observational bias. If only periods measured with *TESS* are considered (dashed light-blue line), a KS-test provides weak indications for the period distribution being different to those of non-magnetic white dwarfs (p -value = 0.027). The incomplete sample of magnetic white dwarfs within 20 pc (dotted dark-blue line) also contains slightly shorter periods compared to non-magnetic white dwarfs.

Table 2. Two-sided Kolmogorov–Smirnov test results for the different samples: all magnetic white dwarfs (Table C1 and *TESS* targets from Table 3), *TESS* targets from Table 3, and white dwarfs within 20 pc compared to non-magnetic white dwarfs (Table C2). The unbiased sample of periods measured with *TESS* confirms previous indications that magnetic white dwarfs rotate on average faster than non-magnetic ones.

Sample 1	Sample 2	KS statistic	p -value
Magnetic	Non-magnetic	0.590	3.761×10^{-7}
20 pc	Magnetic	0.333	0.300
<i>TESS</i>	Magnetic	0.354	0.306
20 pc	Non-magnetic	0.5	0.042
<i>TESS</i>	non-magnetic	0.541	0.027
Sample	Median period	Average period	St. dev.
	(h)	(h)	(h)
Non-magnetic	29.70	32.13	24.04
Magnetic	2.44	20.23	63.17
20 pc	6.19	11.61	12.22
<i>TESS</i>	6.22	10.70	10.37
Magnetic (no mergers)	3.14	23.11	67.04

driven dynamo, and the origin of magnetic fields in white dwarfs in general, it is of fundamental importance to compare spin periods of non-magnetic and magnetic white dwarfs.

In order to perform the comparison of spin periods of non-magnetic and magnetic white dwarfs, we need to consider possible observational biases. The rotation periods of non-magnetic white dwarfs have been measured through asteroseismology. The 36 non-magnetic white dwarfs with asteroseismological measurements of

their rotation period are listed for completeness in Table C2. They cover the mass range from 0.45 to $0.88 M_{\odot}$, which covers the peak of the mass distribution of isolated white dwarfs. Pulsating white dwarfs are located in the instability strip, and therefore cover a rather small range of temperatures (between $10\,000$ and $14\,000$ K, depending slightly on the surface gravity). However, this bias with respect to temperature (and therefore age) is unlikely to affect the distribution of spin periods given the absence of an efficient braking mechanism such as, for example, magnetic braking.

On the other hand, given that magnetic white dwarfs within 20 pc are on average older (Bagnulo & Landstreet 2022), we need to consider that they may have experienced spin-down through the same process assumed for pulsars, that is, magnetic dipole radiation. This means that the initial spin periods of magnetic white dwarfs could have been shorter than the ones we measure today. To explore this possibility, we calculated the initial spin period of the white dwarf using equation (2) in section 3.3 from Williams, Hermes & Vanderbosch (2022), which requires the mass, radius, and the measured spin period (Table 3). We then integrated the equation over the cooling age and found that for our targets, the initial spin period was not significantly different (less than 5 per cent shorter) from the one currently measured, except for WD 0011–134, which has a short period of 0.74 h and is more than 4 Gyr old. This white dwarf might have been fast spinning initially. However, there is strong evidence for the late appearance of the magnetic field in white dwarfs (Bagnulo & Landstreet 2021; Schreiber et al. 2021a), which means that white dwarfs we observe today as magnetic white dwarfs, very likely did not emit magnetic dipole radiation throughout their entire cooling age but only since the magnetic field emerged. Therefore, reconstructing initial spin periods remains impossible as long as we do not understand the mechanisms responsible for the magnetic fields in white dwarfs.

We are aware of the fact that the rotation rates from photometric variations and those inferred from asteroseismology may be measuring slightly different quantities, i.e. surface and globally averaged rotation rates, respectively (Oliveira da Rosa et al. 2022). These quantities might be slightly different but we expect them to be in general very similar. This assumption seems to be justified as Hermes et al. (2017b) could show for the helium-atmosphere white dwarf PG 0112+104 that the rotation period derived from the light curve (10.17 h) was consistent with the rotational splittings from pulsations which indicate a period of ~ 10 h. We therefore decided to compare the currently measured spin periods of magnetic white dwarfs with that of non-magnetic white dwarfs. Neither the fact that the latter are systematically younger nor that the periods derived from light curves and pulsations measure slightly different quantities affects the conclusions we draw in this paper.

The corresponding cumulative distributions are shown in Fig. 4. We used the Kolmogorov–Smirnov test to statistically evaluate possible differences between the samples. The results of this test are listed in Table 2. The full sample of measured periods for magnetic white dwarfs is clearly different to the rotation rates of non-magnetic white dwarfs with a high significance ($p \simeq 3.76 \times 10^{-7}$). As the periods of the magnetic sample are potentially biased towards short periods (mostly coming from ground-based observations), this result does not allow us to derive strong conclusions.

TESS provides continuous light curves for long enough time spans that in principle allow us to measure periods of several days and therefore this sample is not biased against periods as long as those measured for non-magnetic white dwarfs. The range of periods we measured with *TESS* still appears to be systematically shorter than that of non-magnetic white dwarfs. While the latter cover periods

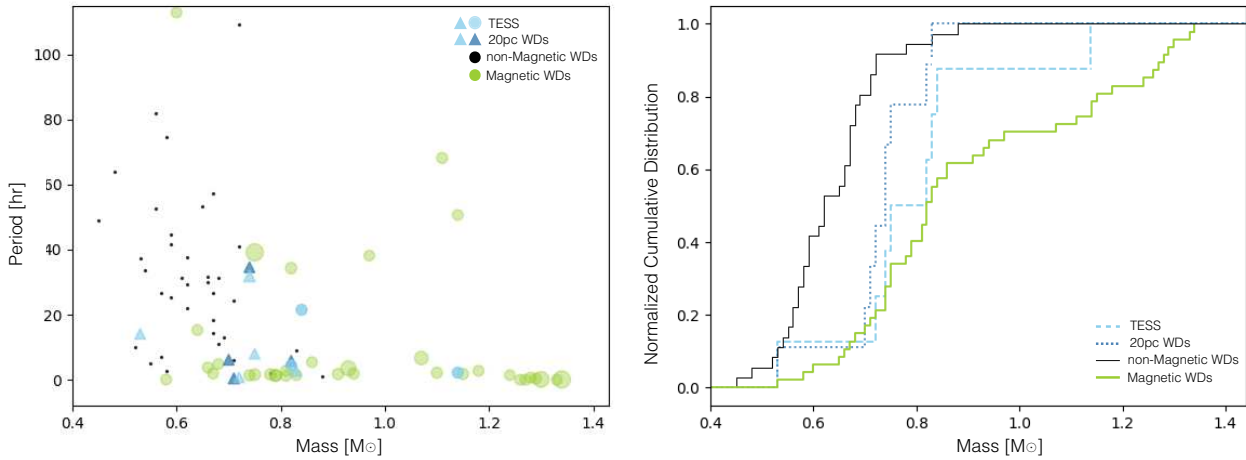


Figure 5. Left: Rotation periods as a function of white dwarf mass for non-magnetic white dwarfs (black dots) from Table C2, and magnetic white dwarfs (green circles) from Tables C1 and 1. The magnetic white dwarfs with periods measured from *TESS* light curves (light blue circles and triangles) and those within 20 pc (dark blue triangles) have, on average, shorter periods than non-magnetic white dwarfs measured from pulsations. Both samples share the light blue triangles, as some of the white dwarfs in the 20 pc sample were observed with *TESS*. Right: Cumulative distributions of the masses of magnetic and non-magnetic white dwarfs. Both, the *TESS* (dashed light-blue line) and the 20 pc sample (dotted dark-blue line) contains slightly more massive white dwarfs than the sample of non-magnetic white dwarfs (solid black line). This difference is statistically significant in both cases ($p = 0.0005$ and $p = 0.0008$), which is consistent with the fact that magnetic white dwarfs in the 20 pc sample are slightly more massive than the non-magnetic ones (Bagnulo & Landstreet 2021).

from 0.33 to 2.34 d, the *TESS* periods we present here range from 0.01 to 0.88 d. The KS tests comparing the periods of non-magnetic white dwarfs with those we measured here confirms these differences (the p -value is reaching 2σ significance). The median and average values further confirm the impression that magnetic white dwarfs rotate on average faster than non-magnetic white dwarfs (Table 2).

Our measurements, however, do not allow us to draw strong conclusions. First, our samples are simply rather small. To provide further evidence for our findings, measuring the rotation periods of all magnetic white dwarfs in the 20 pc sample, e.g. through polarimetry, therefore represents a necessary next step which, unfortunately, requires relatively large amounts of large-telescope observing time. Secondly, as long as we do not understand what is causing the photometric variations in magnetic white dwarfs, we cannot fully exclude that the amplitude of the variations depends on the spin period which would introduce a bias in the distribution of periods.

3.3 Relation between rotation and white dwarf mass

As a first step to evaluate possible dependencies on the white dwarf mass, we plot the cumulative distributions of the white dwarf masses of all previously discussed samples in the right panel of Fig. 5. Previously measured spin periods cover a mass range that is very different to that of typical white dwarfs. The mass distributions of this magnetic white dwarf sample (median: $0.82 M_{\odot}$) and that of the non-magnetic white dwarfs (median: $0.62 M_{\odot}$) are clearly different. In contrast, the 20 pc and the *TESS* sample represent the first ones covering spin periods of more typical white dwarf masses (medians: $0.74 M_{\odot}$ and $0.78 M_{\odot}$, respectively).

However, even both these samples show a tendency towards larger white dwarf masses compared to the sample of single non-magnetic white dwarfs. This reflects the fact that magnetic white dwarfs in the 20 pc sample seem to be slightly more massive than non-magnetic white dwarfs as already mentioned by Bagnulo & Landstreet (2021). According to KS-tests, this difference in masses for both the 20 pc sample ($p = 0.0008$) and the smaller *TESS* sample ($p = 0.0005$).

In the left panel of Fig. 5 we show the rotation period as a function of white dwarf mass for non-magnetic and magnetic white dwarfs. In the 20 pc and *TESS* sample we find white dwarfs with masses exceeding $0.75 M_{\odot}$ to have short periods very similar to what Kawaler (2015) and Hermes et al. (2017a) found for the only three non-magnetic white dwarfs in this mass range.

However, as we shall see, a tendency towards shorter spin periods for larger masses seen in the sample of non-magnetic white dwarfs (but indicated by just three systems) is in general not obvious in magnetic white dwarfs. For white dwarfs exceeding $0.85 M_{\odot}$, spin periods are only known for magnetic white dwarfs. Several very massive and magnetic white dwarfs rotate fast, i.e. with spin periods of minutes. Such typically larger masses and short rotation periods are expected for white dwarf mergers (Schwab 2021) and are entirely absent in the 20 pc sample, i.e. they are rare and largely over-represented in Fig. 5. There are, however, also four magnetic white dwarfs with masses above $0.85 M_{\odot}$ and spin periods of the order of days (one of them is not shown in the figure because its period is longer than 400 h).

In order to test for dependencies of the spin periods on white dwarf masses, we again used cumulative distributions and the KS-test. In the left panel of Fig. 6 we separate the magnetic white dwarfs into samples of normal mass white dwarfs ($\leq 0.85 M_{\odot}$) and massive white dwarfs ($> 0.85 M_{\odot}$) and compare the cumulative distributions. In the right panel of Fig. 6 we compare the same distributions but this time we excluded the obvious merger products which reduces the number of stars in the massive white dwarf sample and the full sample of magnetic white dwarfs by six. There is no significant difference in spin periods for different masses (p -values for all comparisons exceed $p = 0.33$). This result does not depend on the (admittedly arbitrary) value at which we separate high and low-mass white dwarfs. Using e.g. $0.75 M_{\odot}$ or $0.8 M_{\odot}$ instead of $0.85 M_{\odot}$ provides essentially the same results. However, we again advocate caution with the above results because we are dealing with low-number statistics. More spin period measurements are clearly needed before solid conclusions can be drawn.

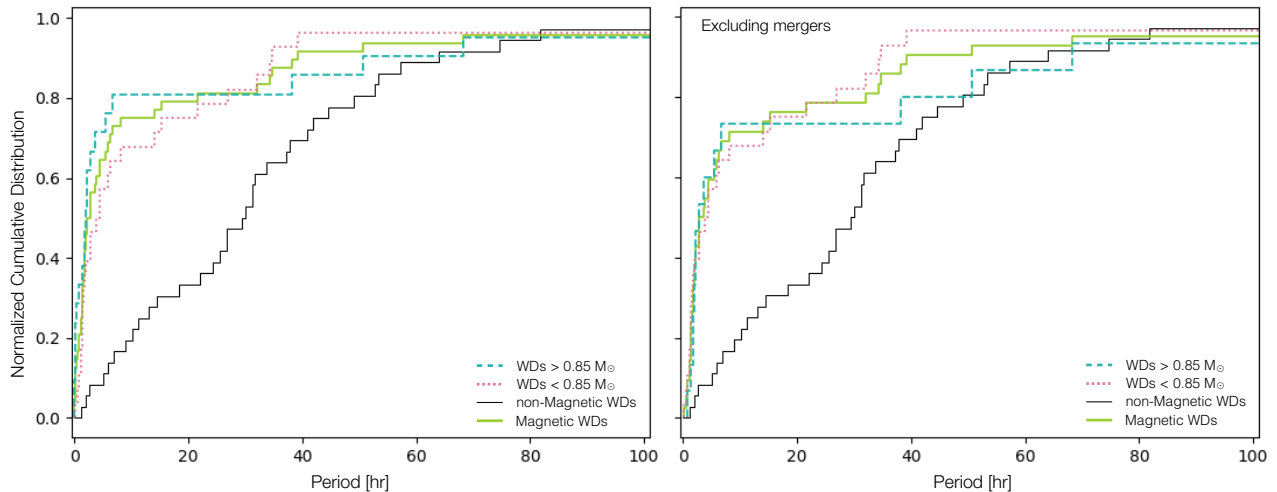


Figure 6. Cumulative period distributions of magnetic and non-magnetic white dwarfs. Left: non-magnetic white dwarfs (solid black line) are compared with the magnetic ones separated in three different samples: all magnetic white dwarfs (Tables C1 and 3, solid green line), magnetic white dwarfs with masses below $0.85 M_{\odot}$ (dotted pink line), and massive magnetic white dwarfs ($\geq 0.85 M_{\odot}$, dashed blue line). Right: The same samples as in the left panel, but removing white dwarfs that very likely formed throughout mergers (rotational periods shorter than 0.38 h and masses larger than $1.25 M_{\odot}$). No indications for a relation between spin period and white dwarf mass can be identified especially if white dwarfs that likely formed through mergers are eliminated.

3.4 Dependencies on spectral type

DZ white dwarfs show metal absorption lines which are indicative of ongoing (or recent) accretion events (e.g., Jura 2003; Gänsicke et al. 2006; Vanderburg et al. 2015; Gänsicke et al. 2019). Intriguingly, Kawka et al. (2019) and Hollands et al. (2017) discovered a large number of magnetic white dwarfs among samples of cool metal-polluted white dwarfs and claimed that there might be an increase in magnetism among these white dwarfs (see also Bagnulo & Landstreet 2019). This alleged increase in magnetism among metal-polluted white dwarfs motivated Schreiber et al. (2021b) to speculate that faster rotation, generated by the accretion of planetary debris, could trigger the crystallization and rotation-driven dynamo. Indeed, accretion can easily reduce the spin period from a few days to a few hours (Schreiber et al. 2021b, their fig. 2).

However, there are two fundamental arguments against a relation between metal pollution and magnetism. First, and most importantly, the volume-limited sample provided by Bagnulo & Landstreet (2021) shows that there most likely is no increase in magnetism for metal-polluted white dwarfs. Of the 26 metal-polluted white dwarfs within 20 pc of the Sun, only six are magnetic. This corresponds to a fraction of 0.23 ± 0.08 magnetic white dwarfs among metal-polluted white dwarfs which is identical to the overall fraction of magnetic white dwarfs among cool ($T_{\text{eff}} \leq 15000$ K) white dwarfs in the 20 pc sample ($33/139 = 0.24 \pm 0.035$). In other words, there are no indications for an increase in magnetism among metal-polluted white dwarfs in this volume-limited sample.

Secondly, if a cold and old DA white dwarf is observed today, accretion of planetary debris onto this white dwarf might have occurred in the past and therefore could have increased the white dwarf’s rotation rate. It is therefore unclear if metal-polluted white dwarfs should indeed rotate faster on average than white dwarfs of other spectral types. If the accretion of planetary debris occurs in relatively short episodes on a large number of white dwarfs over a long period of time, one would rather expect a relation between rotation rate and age.

We here present measurements of the rotation periods of metal-polluted white dwarfs which complement the rough estimate of 18.5 h for WD G29-38 by Thompson et al. (2010). The two clearly variable light curves we measured with SPECULOOS show that these two metal-polluted white dwarfs have periods of the order of a few hours. Our SPECULOOS observations show that LSPM J0107+2650 has a period of 4.8 h while for WD 2138-332 we estimate a period in the range of 4–12 h. As we observed several magnetic DZ white dwarfs with SPECULOOS the two measurements we performed with SPECULOOS are potentially biased towards short periods. Given that in addition both targets have periods typical for magnetic white dwarfs, we conclude that the currently available data does not provide evidence for faster rotation among metal-polluted white dwarfs (nor against it).

While there seems to be no strong evidence for a dependence of the spin period on the spectral types, we observe indications for a relation between spectral type and amplitude of the detected photometric variations. In Table 1 we list the amplitudes of the measured variations for the white dwarfs presented in this work. In Table 3, we list the white dwarfs according to their amplitudes, from smallest to largest, along with their stellar parameters from the literature.

While the four DA white dwarfs show variations with an amplitude of ~ 0.3 – 0.8 percent, the DZ and DC white dwarfs in our sample show variations with larger amplitudes ranging from 0.8 to 10 percent. If confirmed by analysing larger samples, this finding might indicate that the variations are produced by different effects in the different spectral types.

4 DISCUSSION

We presented periodic light-curve variations of eleven magnetic white dwarfs and interpret the periodicity as reflecting the spin period of the white dwarfs. We compared these measurements with spin periods of magnetic and non-magnetic white dwarfs from the literature and obtain the following results: (i) The spin periods of magnetic white dwarfs are shorter than that of non-magnetic white

Table 3. Stellar parameters from *TESS* and *SPECULOOS* targets obtained from literature. The white dwarf spectral types, temperatures, masses, log g , cooling age, and magnetic field magnitude have been taken from Bagnulo & Landstreet (2021, 2022) for nine of our targets. The masses for the *TESS* white dwarf with distance larger than 20 pc were obtained from Gentile Fusillo et al. (2019). For the metal-polluted white dwarf LSPM J0107+2650 whose parameters are listed in Hollands et al. (2017), and for WD 2359-434 whose parameters were obtained from Bagnulo & Landstreet (2019). The listed distances were obtained from the *Gaia* catalogue (Gaia Collaboration 2021). The targets are sorted based on the measured amplitude of their light curves.

Name	Type	Temperature (K)	Mass (M_{\odot})	log g	Age (Gyr)	Magnetic field (MG)	Distance (pc)	Period (h)	Normalized amplitude
<i>TESS</i>									
WD 0011-134	DAH	5855	0.72	8.22	4.1	12	18.56 ± 0.01	0.736 ± 0.007	0.0033 ± 0.0004
WD 0009+501	DAH	6445	0.75	8.25	3.24	0.25	10.87 ± 0.01	4.0086 ± 0.0001	0.0034 ± 0.0003
WD 2359-434	DAH	8390	0.83	8.37	1.83	0.10	8.33 ± 0.01	2.694 ± 0.002	0.0037 ± 0.0001
WD 0011-721	DAH	6340	0.53	7.89	1.66	0.37	18.79 ± 0.01	14.13 ± 0.38	0.0038 ± 0.0003
WD J075328.47–511436.98	DAH	9280	0.84	8.39	–	19	32.71 ± 0.02	21.51 ± 0.01	0.0062 ± 0.0005
WD J171652.09–590636.29	DAH	8600	0.82	8.37	–	0.7	29.83 ± 0.03	4.4398 ± 0.0003	0.0080 ± 0.0001
WD 0912+536	DCH	7170	0.74	8.27	2.48	100	10.27 ± 0.01	31.93 ± 0.13	0.0189 ± 0.0001
WD 0041-102	DBAH	21 341	1.14	–	0.35	20	31.1 ± 0.041	2.19 ± 1.09	0.0327 ± 0.0003
<i>SPECULOOS</i>									
WD 2138-332	DZH	6908	0.6	8.05	1.72	0.05	16.11 ± 0.01	6.19 ± 0.05	0.008 ± 0.001
LSPM J0107+2650	DZ	6190	0.68	–	2.9	3.37	71.96 ± 1.16	4.82 ± 0.29	0.113 ± 0.01

Note. For the white dwarf WD 0009+501, the table shows the spin period measured by *TESS*, which is half of the real spin period previously obtained by spectropolarimetric observations in Valyavin et al. (2005).

dwarfs but larger unbiased samples are needed to confirm this. We note that the spin periods have been measured in an unbiased way for only six of the 33 magnetic white dwarfs within 20 pc, and therefore definite conclusions cannot be drawn. (ii) Massive ($\gtrsim 0.85 M_{\odot}$) magnetic white dwarfs rotate on average slightly faster than lower mass magnetic white dwarfs. However, this difference disappears if strong merger candidates (very fast-rotating massive white dwarfs) are eliminated from the sample. A general trend for decreasing rotation periods with white dwarf mass can therefore not be established. Only the obvious merger candidates, i.e. very massive ($> 1.25 M_{\odot}$) and fast rotating (of the orders of minutes) white dwarfs stand out. (iii) We estimated rotation rates for two metal-polluted white dwarfs and find that both of them have periods of a few hours. Given that the previously published estimate of 18.5 h for WD G29-38 (Thompson et al. 2010) can be considered a rather rough estimate, these are the first robust measurements of rotation periods of metal-polluted white dwarfs. (iv) We found the amplitudes of the variations to depend on the spectral type of the white dwarfs, with variations in DA white dwarfs showing smaller amplitudes than those of DZ or DC white dwarfs. However, a larger homogeneous sample of light curves of magnetic white dwarfs is needed to confirm this potential trend.

In what follows we discuss how robust our findings are and relate them to theories suggested for the origin of magnetic fields in white dwarfs.

4.1 Spin periods and the crystallization dynamo

Investigating the origin of magnetic fields in white dwarfs in close binary stars and based on the early work by Isern et al. (2017), Schreiber et al. (2021a) assumed fast rotation to be a necessary ingredient for the dynamo to work. The proposed scenario assumes that white dwarfs in detached post-common envelope binaries are born without a magnetic field and that only when a crystallizing white dwarf is spun-up by accretion of angular momentum in semi-detached cataclysmic variables does the crystallization and rotation-driven dynamo generates a strong magnetic field. If the field is strong enough, it can connect with the field of the secondary star and transfer spin angular momentum to the orbit. This can cause the binary to

detach for a relatively short period of time. The proposed scenario is very attractive as it can explain several otherwise inexplicable observations: the absence of strongly magnetic white dwarfs in young detached post common envelope binaries (Liebert, Bergeron & Holberg 2003), the population of old and close to Roche-lobe filling post common envelope binaries (Parsons et al. 2021), the existence of the fast spinning white dwarf radio pulsar AR Sco (Marsh et al. 2016), the absence of X-ray bright polars in globular clusters (Belloni et al. 2021), and the fact that all but one white dwarf in close detached double white dwarf binaries are not magnetic (Schreiber et al. 2022).

However, as we have mentioned previously, the only magnetic white dwarfs that rotate with spin periods of the order of minutes are very massive and are consistent with being formed through stellar mergers. This implies that the fast rotation suggested by Isern et al. (2017) and Schreiber et al. (2021a) is very unlikely to generally play a role in the magnetic field generation. At the very best fast rotation may increase the strength of generated fields.

Recently, Ginzburg et al. (2022) showed that convection in crystallizing white dwarfs is slower than previously estimated by Isern et al. (2017) which translates to slower rotation rates being required for the dynamo to work. Ginzburg et al. (2022) also estimated the time-scale for the generated magnetic field to appear on the surface of the white dwarf to be between $\simeq 0.1$ and 1 Gyr depending on the extension of the carbon enriched convection zone. The results presented in this paper might be consistent with the slow-convection dynamo playing a role in the magnetic field generation in white dwarfs. We found that seven of nine periods measured with *TESS* of magnetic white dwarfs rotate with periods of just a few hours and/or have only relatively weak magnetic fields which could be consistent with the slow convection dynamo.

However, it also becomes immediately clear that the dynamo cannot be responsible for all magnetic fields in white dwarfs. In particular, the DCH white dwarf WD 0912+536 has a very strong field ($\gtrsim 100$ MG), a typical white dwarf mass, and a spin period significantly longer than one day (similar to that of longer period non-magnetic white dwarfs). Furthermore, the DAH white dwarf WD J075328.47–511436.98 rotates with a spin period exceeding 20 h and hosts a magnetic field with a strength of 19 MG which is

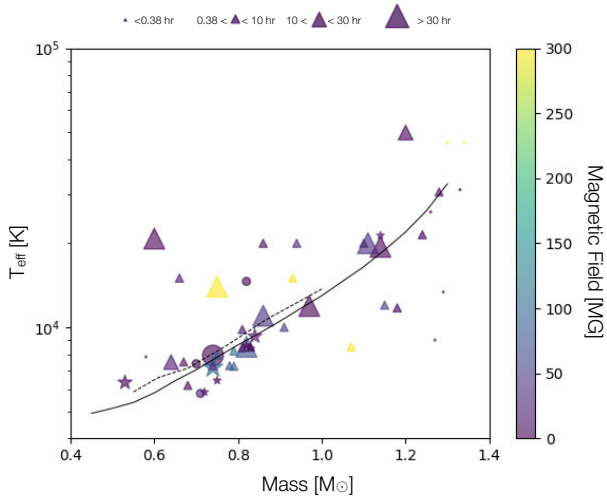


Figure 7. Mass-temperature distribution of magnetic white dwarfs. White dwarfs with periods measured from *TESS* light curves are represented by stars, white dwarfs with measured periods and within 20 pc from Table C1 are marked as filled circles, and the white dwarfs from Table C1 are represented by triangles. Colours show the magnetic field strength with a maximum of 300 MG while the size of the objects (scale on the top of the image) represents different ranges of the rotational period of the white dwarfs. The solid and dashed lines provide the temperature limits for the onset of crystallization according to Bédard et al. (2020) and Salaris et al. (2010), respectively.

also difficult to explain with the dynamo (see Ginzburg et al. 2022; their fig. 4).

To further investigate to which degree the proposed dynamo may contribute to the magnetic field generation in white dwarfs, we compare the available information, white dwarf mass, rotation period, field strengths, and effective temperature of magnetic white dwarfs with the predictions of the dynamo scenario in Fig. 7. If the crystallization and rotation-driven dynamo represents an important channel for magnetic field generation in white dwarfs, one would expect to see an accumulation of magnetic white dwarfs with crystallizing cores rotating relatively fast or a relation between rotation period and field strength.

Indeed, most magnetic white dwarfs have periods of a few hours or less, magnetic field strength of less than a few MG and accumulate in the lower left corner of Fig. 7, i.e. have low temperatures and typical white dwarf masses. It also seems that a significant number of magnetic white dwarfs cluster around the onset of crystallization. Although some of them rotate too slowly to generate their magnetic field through the dynamo, this clustering might imply that crystallization plays a role in the magnetic field generation of some white dwarfs. Also the magnetic white dwarfs in the *TESS* and 20 pc sample (stars and circles) are mostly close to the crystallization limit but some of them rotate very slowly yet host strong fields. If we include magnetic white dwarfs from the literature (triangles), it further becomes obvious that magnetic white dwarfs rotating relatively fast can be found above the temperature limit for the onset of crystallization as well as below. This suggests that the dynamo might be responsible for a fraction of the observed magnetic fields in single white dwarfs but is clearly unable to explain all of them.

4.2 Fast spinning massive white dwarfs and the merger channel

The only crystal clear tendency that can be seen in Fig. 7 is the existence of very fast rotators among high-mass white dwarfs, i.e.

we see evidence for the merger channel (García-Berro et al. 2012) producing magnetic white dwarfs.

Our literature search provided a relatively large number of high-mass white dwarfs with short spin periods. These white dwarfs are absent in the 20 pc sample (Bagnulo & Landstreet 2021) and are therefore rare (Gentile Fusillo et al. 2021). There is an increasing amount of evidence that these magnetic high-mass white dwarfs are the product of mergers as suggested early by García-Berro et al. (2012). Kilic et al. (2023) showed that 40 per cent of high-mass white dwarfs are magnetic which exceeds the 20 per cent found in volume-limited samples (Bagnulo & Landstreet 2021). This finding is in agreement with Bagnulo & Landstreet (2022) who find that in high-mass white dwarfs, magnetic fields are extremely common, very strong, and appear immediately in the cooling phase while lower mass white dwarfs become magnetic close to the onset of crystallization. Further evidence for the generation of magnetic fields through mergers is provided by Pelisoli et al. (2022) who found evidence for the three known magnetic hot sub-dwarfs to be the product of a merger.

Theoretical simulations of the merger process predict the remnant to have very short spin periods of just $\simeq 10\text{--}20$ min (Schwab 2021). This prediction fits with the most massive white dwarfs that are rotating with periods of this order (we used a rather arbitrary limit of 0.38 h in Fig. 7). We, therefore, conclude that at least these fast-spinning, strongly magnetic, and very massive white dwarfs are the product of mergers. However, it seems that not all mergers produce strongly magnetic white dwarfs. Hollands et al. (2020) found a massive white dwarf that is likely the product of a merger and derived an upper limit on the field strength of only 50 kG.

The magnetic white dwarfs in the mass range of $\sim 0.8\text{--}1.2$ that do not spin with periods of minutes, show spin periods similar to that of less massive magnetic white dwarfs. This means, the spin periods of these white dwarfs alone do not provide evidence for them emerging from a different channel than the lower mass white dwarfs. In other words, the spin periods alone do not provide indications that these white dwarfs might be mergers as well.

4.3 Constraints on magnetic field generation in white dwarfs

Of the mechanisms suggested for magnetic field generation, the merger channel is the most convincing and the only one that can count on clear observational evidence. However, only very few white dwarfs are produced through this channel which is clearly illustrated by the complete absence of such white dwarfs in the 20 pc sample (Bagnulo & Landstreet 2021).

Concerning the dominant population of magnetic white dwarfs we know the following: the 20 pc sample established by Bagnulo & Landstreet (2021) shows that in general magnetic fields in white dwarfs appear late, i.e. when the white dwarf has cooled to temperatures similar to the onset of crystallization. This is illustrated by the white dwarfs marked as stars and circles in Fig. 7. In this work, we complemented this result by finding that a significant fraction of these cool nearby white dwarfs rotate fast (periods of a few hours) while others are slowly rotating (longer than 20 h). In addition, we find that on average magnetic white dwarfs rotate faster than non-magnetic white dwarfs. These constraints seem to imply that in general rotation plays a role in the generation of white dwarf magnetic fields but not in all cases.

It could be not just one additional channel to the merger channel but several, and only one of them necessitates relatively fast rotation. The generally late appearance of the magnetic fields could imply that crystallization plays a role or that the fields appear late for a different

reason, e.g. because they were buried following the white dwarf formation. We clearly need a larger sample of well characterized magnetic white dwarfs and new theoretical ideas to finally understand the formation of magnetic fields in white dwarfs.

4.4 Magnetic white dwarfs in binaries

The absence of strongly magnetic white dwarfs in young post-common envelope binaries was one of the main motivations for the development of the crystallization and rotation-driven dynamo (Schreiber et al. 2021a). This absence of young magnetic white dwarfs in close binaries is consistent with the absence of strongly magnetic single white dwarfs in the 20 pc sample (Bagnulo & Landstreet 2021). Whether the generally late appearance of magnetic fields in white dwarfs is caused by a dynamo that requires crystallization or if the magnetic field appears late for another reason remains an open question.

In any case, whether the magnetic field is generated late due to a dynamo (that does depend on rotation) or appears late in the evolution of a white dwarf for another reason (e.g. because it was buried), the evolutionary sequence suggested by Schreiber et al. (2021a) for white dwarf binaries (i.e. magnetic field appearance/generation during the CV phase, connection with the field of the secondary, angular momentum transfer to the orbit, cessation of mass transfer, synchronization, re-start of mass transfer) remains a promising scenario to explain the observations of magnetic white dwarfs in post common envelope binaries and CVs.

The situation for double white dwarfs is similar. As shown by Schreiber et al. (2022), only one magnetic white dwarf is known in these systems (which is close to the crystallization boundary and rapidly rotating). If rotation does not play a crucial role in the magnetic field generation, cool white dwarfs in close double white dwarfs should develop magnetic fields. In the 20 pc sample the occurrence rate of magnetism increases for effective temperatures in the range of 4 000 – 8 000 K (Bagnulo & Landstreet 2021; their fig. 2) while the vast majority of both components in double white dwarfs are hotter. It might therefore be that in both populations, close double white dwarfs, and post common envelope binaries with main sequence star companion, the late appearance of magnetic fields has not yet been observed.

Further searches for magnetism in cool white dwarfs that are part of post-common envelope binaries or double white dwarfs would significantly help us to settle open questions. If rotation is not a key ingredient for the appearance of magnetic fields, we should find magnetic white dwarfs in detached double white dwarfs and among post-common envelope binaries that contain cool white dwarfs and that are not close to Roche-lobe filling. The latter does not seem to be the case (Parsons et al. 2021), but the sample size is still small and heavily biased towards systems that are close to Roche-lobe filling as the magnetic fields are detected through cyclotron emission via wind accretion. Further observations, especially of systems containing the coolest white dwarfs are certainly required (but might be challenging).

5 CONCLUSIONS

The 20 pc sample provided by Bagnulo & Landstreet (2021) showed that white dwarfs become magnetic when they are older, typically with ages exceeding 2 Gyr (see also Bagnulo & Landstreet 2022), reaching effective temperatures close to the crystallization limit. While detached post-common envelope binaries are hardly ever

magnetic, a large number of their descendants, semidetached cataclysmic variables turned out to host a magnetic white dwarf. In other words, there is clear observational evidence for the late appearance of magnetic fields in white dwarfs. Based on this finding and the early work by Isern et al. (2017), a crystallization and rotation-driven dynamo has been proposed for the origin of magnetic fields in white dwarfs (Schreiber et al. 2021a; Ginzburg et al. 2022).

We presented measurements of the spin periods of eight magnetic white dwarfs using *TESS* light curves and found that their spin periods are similar to those of previously identified magnetic white dwarfs and shorter than that of non-magnetic white dwarfs. Four of the periods we measured agree with previously measured periods and in one of them the *TESS* period is half the real period. One white dwarf in our sample has magnetic field strengths of ~ 100 MG but a long rotation rate of 32 h. This result indicates that fast rotation plays a role in the magnetic field generation in general but is not always required.

In a sample of magnetic white dwarfs compiled from the literature, some massive white dwarfs entirely consistent with being merger products stand out. In the remaining systems, we do not find evidence for a dependence of spin period on white dwarfs mass but a larger and/or complete volume-limited sample of magnetic white dwarfs is needed to confirm this impression.

The crystallization and rotation-driven dynamo might be responsible for a fraction of the magnetic fields in white dwarfs. If it is, a third mechanism to the dynamo and mergers would probably be required. Alternatively, the proposed dynamo does not play a role but just one channel (complementing the magnetic white dwarfs resulting from mergers), that for some reason leads to the late appearance of magnetic fields and on average shorter spin periods, is responsible for the generation of most magnetic fields in white dwarfs. Independent of the reasons for the late appearance of magnetic fields, the new evolutionary sequence suggested by Schreiber et al. (2021a) for white dwarfs in binaries remains plausible.

ACKNOWLEDGEMENTS

We thank the anonymous referee for their comments, which have helped us to improve the paper. We thank the Kavli Institute for Theoretical Physics (KITP) for hosting the program ‘White Dwarfs as Probes of the Evolution of Planets, Stars, the Milky Way and the Expanding Universe’. This research was supported in part by the National Science Foundation under Grant No. NSF PHY-1748958. MSH acknowledges support through a postdoc fellowship from the DGIIE (General Direction of Research, Innovation and Undertaking) of the UTFSM. MRS acknowledges support by ANID, Millennium Science Initiative Program – NCN19-171, and FONDECYT (grant 1221059). OT was supported by FONDECYT grant 3210382. JDL acknowledges the financial support of the Natural Sciences and Engineering Research Council of Canada (NSERC), funding reference number 6377–2016. SGP acknowledges the support of an STFC Ernest Rutherford Fellowship. For the purpose of open access, the author has applied a creative commons attribution (CC BY) licence to any author accepted manuscript version arising.

DATA AVAILABILITY

SPECULOOS photometry is available at the data archive of the European Southern Observatory under ESO programme 0108.A9010(C) and the analysed *TESS* data are publically available.

REFERENCES

- Achilleos N., Wickramasinghe D. T., 1989, *ApJ*, 346, 444
- Achilleos N., Wickramasinghe D. T., Liebert J., Saffer R. A., Grauer A. D., 1992, *ApJ*, 396, 273
- Angel J. R. P., 1977, *ApJ*, 216, 1
- Angel J. R. P., Borra E. F., Landstreet J. D., 1981, *ApJS*, 45, 457
- Angel J. R. P., Landstreet J. D., 1971, *ApJ*, 165, L71
- Augustson K., Mathis S., Brun A. S., Toomre J., 2016, in 19th Cambridge Workshop on Cool Stars, Stellar Systems, and the Sun (CS19). Cambridge Workshop on Cool Stars, Stellar Systems, and the Sun. p. 29
- Aurière M. et al., 2007, *A&A*, 475, 1053
- Bagnulo S., Landstreet J. D., 2019, *A&A*, 630, A65
- Bagnulo S., Landstreet J. D., 2021, *MNRAS*, 507, 5902
- Bagnulo S., Landstreet J. D., 2022, *ApJ*, 935, L12
- Barstow M. A., Jordan S., O'Donoghue D., Burleigh M. R., Napiwotzki R., Harrop-Allin M. K., 1995, *MNRAS*, 277, 971
- Bédard A., Bergeron P., Brassard P., Fontaine G., 2020, *ApJ*, 901, 93
- Bell K. J., Hermes J. J., Bischoff-Kim A., Moorhead S., Montgomery M. H., Østensen R., Castanheira B. G., Winget D. E., 2015, *ApJ*, 809, 14
- Belloni D., Schreiber M. R., 2020, *MNRAS*, 492, 1523
- Belloni D., Schreiber M. R., Salaris M., Maccarone T. J., Zorotovic M., 2021, *MNRAS*, 505, L74
- Bergeron P., Leggett S. K., Ruiz M. T., 2001, *ApJS*, 133, 413
- Bergeron P., Saffer R. A., Liebert J., 1992, *ApJ*, 394, 228
- Bevington P. R., 1969, *Data Reduction and Error Analysis for the Physical Sciences*. McGraw-Hill, New York
- Blackett P. M. S., 1947, *Nature*, 159, 658
- Bognár Z., Paparó M., Molnár L., Pápics P. I., Plachy E., Verebélyi E., Sódor Á., 2016, *MNRAS*, 461, 4059
- Bradley P. A., 2001, *ApJ*, 552, 326
- Braithwaite J., Spruit H. C., 2004, *Nature*, 431, 819
- Brinkworth C. S., Burleigh M. R., Lawrie K., Marsh T. R., Knigge C., 2013, *ApJ*, 773, 47
- Brinkworth C. S., Burleigh M. R., Wynn G. A., Marsh T. R., 2004, *MNRAS*, 348, L33
- Brinkworth C. S., Marsh T. R., Morales-Rueda L., Maxted P. F. L., Burleigh M. R., Good S. A., 2005, *MNRAS*, 357, 333
- Bues I., Pragal M., 1989, in Wegner G., ed., *Proc. IAU Symp. 328, Colloq. 114: White Dwarfs*. Springer-Verlag, Berlin, New York, p. 329
- Burleigh M. R., Jordan S., Schweizer W., 1999, *ApJ*, 510, L37
- Caiazzo I. et al., 2021, *Nature*, 595, 39
- Castanheira B. G., Kepler S. O., Kleinman S. J., Nitta A., Fraga L., 2013, *MNRAS*, 430, 50
- Charpinet S., Fontaine G., Brassard P., 2009, *Nature*, 461, 501
- Delrez L. et al., 2018, in Marshall H. K., Spyromilio J., eds, *Proc. SPIE Conf. Ser. Vol. 10700, Ground-based and Airborne Telescopes VII*. SPIE, Bellingham, p. 107001I
- Dolez N. et al., 2006, *A&A*, 446, 237
- Dufour P., Fontaine G., Liebert J., Schmidt G. D., Behara N., 2008, *ApJ*, 683, 978
- Dupuis J., Chayer P., Vennes S., Christian D. J., Kruk J. W., 2000, *ApJ*, 537, 977
- Euchner F., Jordan S., Reinsch K., Beuermann K., Gänsicke B. T., 2005, in Koester D., Moehler S., eds, *ASP Conf. Ser. Vol. 334, 14th European Workshop on White Dwarfs*. Astron. Soc. Pac., San Francisco, p. 269
- Farihi J., Hermes J. J., Littlefair S. P., Howarth I. D., Walters N., Parsons S. G., 2023, *MNRAS*, 525, 1097
- Ferrario L., de Martino D., Gänsicke B. T., 2015, *Space Sci. Rev.*, 191, 111
- Ferrario L., Wickramasinghe D. T., Liebert J., Schmidt G. D., Biegging J. H., 1997, *MNRAS*, 289, 105
- Friedrich S., Koenig M., Schweizer W., 1997, *A&A*, 326, 218
- Fu J. N. et al., 2007, *A&A*, 467, 237
- Fu J. N. et al., 2013, *MNRAS*, 429, 1585
- Gaia Collaboration, 2021, *A&A*, 649, A1
- Gänsicke B. T., Marsh T. R., Southworth J., Rebassa-Mansergas A., 2006, *Science*, 314, 1908
- Gänsicke B. T., Rodríguez-Gil P., Gentile Fusillo N. P., Inight K., Schreiber M. R., Pala A. F., Tremblay P.-E., 2020, *MNRAS*, 499, 2564
- Gänsicke B. T., Schreiber M. R., Toloza O., Gentile Fusillo N. P., Koester D., Manser C. J., 2019, *Nature*, 576, 61
- García L. J., Timmermans M., Pozuelos F. J., Ducrot E., Gillon M., Delrez L., Wells R. D., Jehin E., 2022, *MNRAS*, 509, 4817
- García-Berro E. et al., 2012, *ApJ*, 749, 25
- Gentile Fusillo N. P. et al., 2019, *MNRAS*, 482, 4570
- Gentile Fusillo N. P. et al., 2021, *MNRAS*, 508, 3877
- Giammichele N., Fontaine G., Brassard P., Charpinet S., 2016, *ApJS*, 223, 10
- Ginzburg S., Fuller J., Kawka A., Caiazzo I., 2022, *MNRAS*, 514, 4111
- Greenstein J. L., Henry R. J. W., O'Connell R. F., 1985, *ApJ*, 289, L25
- Greiss S., Gänsicke B. T., Hermes J. J., Steeghs D., Koester D., Ramsay G., Barclay T., Townsley D. M., 2014, *MNRAS*, 438, 3086
- Hakala P., Parsons S. G., Marsh T. R., Gänsicke B. T., Ramsay G., Schwöpe A., Hermes J. J., 2022, *MNRAS*, 513, 3858
- Hardy F., Dufour P., Jordan S., 2023, *MNRAS*, 520, 6111
- Hermes J. J. et al., 2015, *MNRAS*, 451, 1701
- Hermes J. J. et al., 2017a, *ApJS*, 232, 23
- Hermes J. J., Kawaler S. D., Bischoff-Kim A., Provencal J. L., Dunlap B. H., Clemens J. C., 2017b, *ApJ*, 835, 277
- Hermes J. J. et al., 2017c, *ApJ*, 841, L2
- Higgins M. E., Bell K. J., 2023, *AJ*, 165, 141
- Hollands M. A. et al., 2020, *Nat. Astron.*, 4, 663
- Hollands M. A., Koester D., Alekseev V., Herbert E. L., Gänsicke B. T., 2017, *MNRAS*, 467, 4970
- Isern J., García-Berro E., Külebi B., Lorén-Aguilar P., 2017, *ApJ*, 836, L28
- Jehin E. et al., 2018, *The Messenger*, 174, 2
- Jura M., 2003, *ApJ*, 584, L91
- Kawaler S. D. et al., 1995, *ApJ*, 450, 350
- Kawaler S. D., 2015, in Dufour P., Bergeron P., Fontaine G., eds, *ASP Conf. Ser. Vol. 493, 19th European Workshop on White Dwarfs*. Astron. Soc. Pac., San Francisco, p. 65
- Kawka A., Briggs G. P., Vennes S., Ferrario L., Paunzen E., Wickramasinghe D. T., 2017, *MNRAS*, 466, 1127
- Kawka A., Vennes S., 2004, in Zverko J., Ziznovsky J., Adelman S. J., Weiss W. W., eds, *The A-Star Puzzle (Vol. 224)*. Cambridge Univ. Press, Cambridge, p. 879
- Kawka A., Vennes S., Ferrario L., Paunzen E., 2019, *MNRAS*, 482, 5201
- Kawka A., Vennes S., Schmidt G. D., Wickramasinghe D. T., Koch R., 2007, *ApJ*, 654, 499
- Kemp J. C., Swedlund J. B., Landstreet J. D., Angel J. R. P., 1970, *ApJ*, 161, L77
- Kepler S. O. et al., 1995, *ApJ*, 447, 874
- Kilic M. et al., 2015, *ApJ*, 814, L31
- Kilic M. et al., 2023, *MNRAS*, 518, 2341
- Kilic M., Kosakowski A., Moss A. G., Bergeron P., Conly A. A., 2021, *ApJ*, 923, L6
- Külebi B., Jordan S., Euchner F., Hirsch H., Löffler W., 2009, *J. Phys. Conf. Ser.*, 172, 012047
- Landstreet J. D., Bagnulo S., Valyavin G., Valeev A. F., 2017, *A&A*, 607, A92
- Lawrie K. A. et al., 2013b, in Krziesiński J., Stachowski G., Moskalik P., Bajan K., eds, *ASP Conf. Ser. Vol. 469, 18th European White Dwarf Workshop*. Astron. Soc. Pac., San Francisco, p. 429
- Lawrie K. A., Burleigh M. R., Dufour P., Hodgkin S. T., 2013a, *MNRAS*, 433, 1599
- Liebert J. et al., 2005, *AJ*, 129, 2376
- Liebert J., 1976, *PASP*, 88, 490
- Liebert J., Angel J. R. P., Stockman H. S., Spinrad H., Beaver E. A., 1977, *ApJ*, 214, 457
- Liebert J., Bergeron P., Holberg J. B., 2003, *AJ*, 125, 348
- Liebert J., Schmidt G. D., Sion E. M., Starrfield S. G., Green R. F., Boroson T. A., 1985, *PASP*, 97, 158
- Liebert J., Smith P. S., Ferrario L., Wickramasinghe D. T., 2015, in Dufour P., Bergeron P., Fontaine G., eds, *ASP Conf. Ser. Vol. 493, 19th European Workshop on White Dwarfs*. Astron. Soc. Pac., San Francisco, p. 493

Lightkurve Collaboration, 2018, Lightkurve: Kepler and TESS time series analysis in Python, Astrophysics Source Code Library, record:1812.013

Lomb N. R., 1976, *Ap&SS*, 39, 447

Maccarone T. J., Kupfer T., Najera Casarrubias E., Rivera Sandoval L., Shaw A., Britt C., van Roestel J., Zurek D., 2024, *MNRAS*, 529, L28

Manser C. J. et al., 2023, *MNRAS*, 521, 4976

Marsh T. R. et al., 2016, *Nature*, 537, 374

Martin B., Wickramasinghe D. T., 1978, *MNRAS*, 183, 533

Maxted P. F. L., Ferrario L., Marsh T. R., Wickramasinghe D. T., 2000, *MNRAS*, 315, L41

Moran C., Marsh T. R., Dhillion V. S., 1998, *MNRAS*, 299, 218

Moss A., Kilic M., Bergeron P., Fergard M., Brown W., 2023, *MNRAS*, 523, 5598

O'Brien M. W. et al., 2023, *MNRAS*, 518, 3055

Oliveira da Rosa G. et al., 2022, *ApJ*, 936, 187

Østensen R. H., Bloemen S., Vučković M., Aerts C., Oreiro R., Kinemuchi K., Still M., Koester D., 2011, *ApJ*, 736, L39

Pala A. F. et al., 2020, *MNRAS*, 494, 3799

Parsons S. G., Gänsicke B. T., Schreiber M. R., Marsh T. R., Ashley R. P., Breedt E., Littlefair S. P., Meusinger H., 2021, *MNRAS*, 502, 4305

Pech D., Vauclair G., 2006, *A&A*, 453, 219

Pelisolì I. et al., 2022, *MNRAS*, 515, 2496

Pelisolì I. et al., 2023, *Nat. Astron.*, 7, 931

Pfeiffer B. et al., 1996, *A&A*, 314, 182

Pshirkov M. S. et al., 2020, *MNRAS*, 499, L21

Putney A., 1997, *ApJS*, 112, 527

Putney A., Jordan S., 1995, *ApJ*, 449, 863

Rebassa-Mansergas A., Ren J. J., Parsons S. G., Gänsicke B. T., Schreiber M. R., García-Berro E., Liu X. W., Koester D., 2016, *MNRAS*, 458, 3808

Reding J. S., Hermes J. J., Clemens J. C., Hegedus R. J., Kaiser B. C., 2023, *MNRAS*, 522, 693

Reding J. S., Hermes J. J., Vanderbosch Z., Dennihy E., Kaiser B. C., Mace C. B., Dunlap B. H., Clemens J. C., 2020, *ApJ*, 894, 19

Regós E., Tout C. A., 1995, *MNRAS*, 273, 146

Reimers D., Hagen H. J., Hopp U., 1999, *A&A*, 343, 157

Reimers D., Jordan S., Koester D., Bade N., Koehler T., Wisotzki L., 1996, *A&A*, 311, 572

Ricker G. R. et al., 2015, *J. Astron. Telesc. Instrum. Syst.*, 1, 014003

Salaris M., Cassisi S., Pietrinferni A., Kowalski P. M., Isern J., 2010, *ApJ*, 716, 1241

Scargle J. D., 1982, *ApJ*, 263, 835

Schmidt G. D., Norsworthy J. E., 1991, *ApJ*, 366, 270

Schmidt G. D., Vennes S., Wickramasinghe D. T., Ferrario L., 2001, *MNRAS*, 328, 203

Schmidt G. D., West S. C., Liebert J., Green R. F., Stockman H. S., 1986, *ApJ*, 309, 218

Schonhut-Stasik J., Stassun K., 2023, *Res. Notes Am. Astron. Soc.*, 7, 18

Schreiber M. R. et al., 2010, *A&A*, 513, L7

Schreiber M. R., Belloni D., Gänsicke B. T., Parsons S. G., Zorotovic M., 2021a, *Nat. Astron.*, 5, 648

Schreiber M. R., Belloni D., Gänsicke B. T., Parsons S. G., 2021b, *MNRAS*, 506, L29

Schreiber M. R., Belloni D., Zorotovic M., Zapata S., Gänsicke B. T., Parsons S. G., 2022, *MNRAS*, 513, 3090

Schwab J., 2021, *ApJ*, 906, 53

Su J., Li Y., Fu J. N., Li C., 2014, *MNRAS*, 437, 2566

Thompson S. E. et al., 2010, *ApJ*, 714, 296

Tout C. A., Wickramasinghe D. T., Liebert J., Ferrario L., Pringle J. E., 2008, *MNRAS*, 387, 897

Tremblay P. E., Fontaine G., Freytag B., Steiner O., Ludwig H. G., Steffen M., Wedemeyer S., Brassard P., 2015, *ApJ*, 812, 19

Valeev A. F. et al., 2015, *Astrophys. Bull.*, 70, 318

Valyavin G., Bagnulo S., Monin D., Fabrika S., Lee B. C., Galazutdinov G., Wade G. A., Burlakova T., 2005, *A&A*, 439, 1099

Valyavin G., Wade G. A., Bagnulo S., Szeifert T., Landstreet J. D., Han I., Burenkov A., 2008, *ApJ*, 683, 466

Vanderburg A. et al., 2015, *Nature*, 526, 546

Wegner G., 1977, *Mem. Soc. Astron. Ital.*, 48, 27

Wickramasinghe D. T., Cropper M., 1988, *MNRAS*, 235, 1451

Wickramasinghe D. T., Ferrario L., 2005, *MNRAS*, 356, 1576

Wickramasinghe D. T., Martin B., 1979, *MNRAS*, 188, 165

Wickramasinghe D. T., Tout C. A., Ferrario L., 2014, *MNRAS*, 437, 675

Williams K. A., Hermes J. J., Vanderbosch Z. P., 2022, *AJ*, 164, 131

Wilson D. J., Toloza O., Landstreet J. D., Gänsicke B. T., Drake J. J., Hermes J. J., Koester D., 2021, *MNRAS*, 508, 561

APPENDIX A: DETAILS ON THE 20 PC TESS SAMPLE

A1 TESS sectors

We provide the lists of *TESS* sectors that we analysed for all targets within 20 pc. This includes white dwarfs with clear photometric variations (see Table A1).

A2 An eclipsing binary contaminating the TESS light curve

During the *TESS* light curves analysis of WD 2150+591, we noticed that the light curves of two sectors showed features resembling that of an eclipsing binary system. We modified the FLUX CONTAMINATION TOOL recently published by Schonhut-Stasik & Stassun (2023) with the aim to obtain the contamination level and G-magnitude of individual sectors in order to analyse this particular case. We compared the resulting G-magnitudes (by sector) with the white dwarf G-magnitude reported in literature. We found that the sectors showing the variations reminiscent of an eclipsing binary (Fig. A1) indeed were dominated by a nearby eclipsing binary star as the average G-magnitude was significantly smaller than that of the white dwarf. Therefore the variations one can find in the *TESS* data base for WD 2150+591 are clearly not produced by the white dwarf.

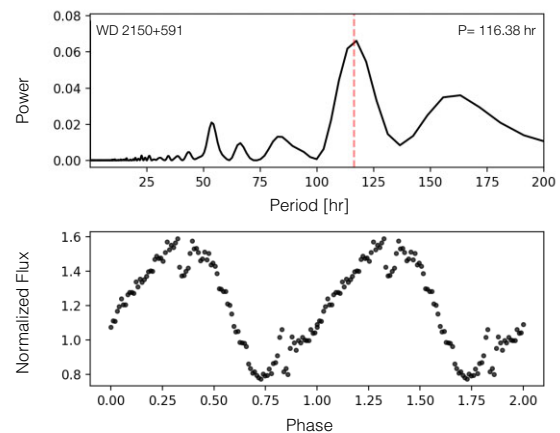


Figure A1. Periodogram and phase-folded *TESS* light curve of WD 2150+591, the closest white dwarf in our sample (8.5 pc). We binned the phase-folded light curve (using 100 bins) to reduce the noise. This white dwarf was observed in five *TESS* sectors, by comparing the G-magnitude of each sector with the magnitude reported in the literature for this white dwarf, we found that two sectors are dominated by the light curve of a nearby eclipsing binary. Here we show the light curve corresponding to sector 56 with a 20 s cadence and a contamination level of 10.5 per cent.

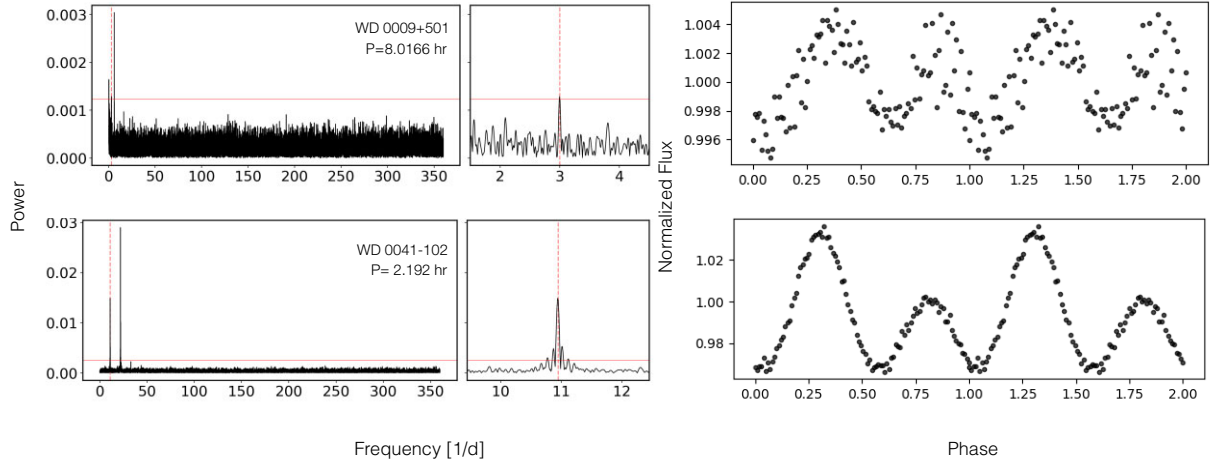


Figure A2. Periodograms (left: up to the Nyquist frequency; middle: zoomed in to the second highest peak) and phase-folded *TESS* light curves (right) of WD 0009+501 and WD 0041-102. The horizontal red line illustrates the false alarm probability level (FAP level) for a probability of 10^{-3} . For both objects the true rotation period is close to the second highest peak in the periodogram. The data of WD 0041-102 was folded over the period indicated by the second highest peak in the periodogram (2.192 h) and we recover the double humped light curve previously reported by Achilleos et al. (1992). In the case of WD 0009+501, the light curve is folded over a period of 8.016 ± 0.083 h, obtained by re-analysing the full spectropolarimetry data set from Valyavin et al. (2005) supplemented with one all-night spectropolarimetry data set in the yet unpublished work of Bagnulo, Landstreet & Valyavin. This magnetic period is almost identical to twice the period of the highest peak in the periodogram (8.017 h) and close to the period indicated by the second highest peak in the periodogram (8.007 h).

Table A1. List of magnetic white dwarfs with *TESS* observations from the 20 pc sample. Targets for which we found clear periodic variations are marked with a ✓ symbol. For these systems, we provide the identification number for all the analysed *TESS* sectors. For those targets without clear variations (marked with ×) we only provide the total number of *TESS* sectors available for each white dwarf. Values in the parenthesis indicate the contamination level for the corresponding sector.

Name	TIC name	Variation	Distance (pc)	FluxCT	Exposure time (s)
WD 0009+501	TIC 201892746	✓	10.87	17(0.0 per cent), 57(4.7 per cent)	120, 20
WD 0011-134	TIC 289712694	✓	18.55	29(0.0 per cent)	120
WD 0011-721	TIC 328029653	✓	18.79	1(10.8 per cent), 27(8.2 per cent), 28(10.4 per cent)	120, 120, 120
WD 0912+536	TIC 251080865	✓	10.27	21(0.0 per cent), 47(0.0 per cent)	120, 20
WD 2359-434	TIC 321979116	✓	8.33	2(0.1 per cent), 29(0.1 per cent)	120, 20
WD 0004+122	TIC 357353518	×	17.45	2(0.0 per cent)	–
WD 0503-174	TIC 169379648	×	19.34	2(11.1 per cent)	–
WD 0121-429	TIC 262548040	×	18.45	4(8.4 per cent)	–
WD 0233-242	TIC 65324009	×	18.46	2(3.4 per cent)	–
WD 0322-019	TIC 279198715	×	16.93	2(3.1 per cent)	–
WD 0548-001	TIC 176670072	×	11.22	2(1.7 per cent)	–
WD 0708-670	TIC 300013123	×	16.96	22(48.9 per cent)	–
WD 0810-353	TIC 145863747	×	11.17	1(28.3 per cent)	–
WD 0816-310	TIC 147018085	×	19.36	1(7.6 per cent)	–
WD 1008+290	TIC 241190677	×	14.73	2(0.0 per cent)	–
WD 1009-184	TIC 52104043	×	18.08	2(1.3 per cent)	–
WD 1036-204	TIC 179299789	×	14.11	2(35.0 per cent)	–
WD 1309+853	TIC 154903874	×	16.47	10(10.9 per cent)	–
WD 1315-781	TIC 448023860	×	19.28	4(28.8 per cent)	–
WD 1532+129	TIC 157110489	×	19.25	1(8.4 per cent)	–
WD 1748+708	TIC 233212451	×	6.21	25(0.0 per cent)	–
WD 1829+547	TIC 390019679	×	17.03	1(0.0 per cent)	–
WD 1900+705	TIC 229797408	×	12.87	1(0.0 per cent)	–
WD 2047+372	TIC 390019679	×	17.58	3(22.9 per cent)	–
WD 2105-820	TIC 403995834	×	16.17	3(5.5 per cent)	–
WD 2150+591	TIC 283414280	×	8.47	2(68.0 per cent)	–
WD 2153-512	TIC 140045537	×	14.85	2(47 per cent)	–

A3 Folding *TESS* data over the real rotation period

For two white dwarfs in our sample, the strongest signal in the periodogram corresponds to half the orbital period. The independently measured period appears as significant second highest peak

in the periodograms. In Fig. A2 we show the *TESS* light curves folded over the true rotation period. In the case of WD 0041-102, this period is identical to the period indicated by the second highest peak in the periodogram. For WD 0009+501, however, the

Table A2. List of magnetic white dwarfs with *TESS* observations from the 40 pc sample. Targets for which we found clear periodic variations are marked with a ✓ symbol. For these systems, we provide the identification number for all the analysed *TESS* sectors. For those targets without clear variations (marked with ×) we only provide the total number of *TESS* sectors available for each white dwarf. Values in the parenthesis indicate the contamination level for the corresponding sector.

Name	TIC name	Variation	Distance (pc)	FluxCT	Exposure time (s)
WD 0041-102	TIC 3888273	✓	31.1	3(0.3 per cent), 30(0.3 per cent)	120, 20
WD 0232+525	TIC 249952539	✓	28.8	18(22.3 per cent), 58(5.2 per cent)	120, 20
WD J075328.47–511436.98	TIC 269071459	✓	32.71	34(59.7 per cent), 35(21.7 per cent), 36(29.7 per cent), 61(17.4 per cent)	120, 120, 120, 20
WD 0316-849	TIC 267166357	×	29.38	4(36.8 per cent)	–
WD 0945+245	TIC 98413819	×	36.20	4(1.4 per cent)	–
WD 1658+440	TIC 115613388	×	31.65	5(4.3 per cent)	–
WD 1704+481.1	TIC 274677205	×	39.45	5(50.2 per cent)	–
WD 2010+310	TIC 92633917	×	30.76	4(56.6 per cent)	–
WD 1008-242	TIC 168071263	×	39.7	1(0.0 per cent)	–
WD J091808.59–443724.25	TIC 75823453	×	28.35	2(65.1 per cent)	–
WD J094240.23–463717.68	TIC 33724884	×	20.47	36(65.5 per cent)	–
WD J171652.09–590636.29	TIC 380174982	×	29.83	2(74.7 per cent)	–
WD J001830.36–350144.71	TIC 63695966	×	35.65	1(4.9 per cent)	–
WD J014240.09–171410.85	TIC 404466241	×	40.0	1(4.0 per cent)	–
WD J025245.61–752244.56	TIC 426018482	×	31.19	6(20.3 per cent)	–
WD J035531.89–561128.32	TIC 197909428	×	32.95	3(0.0 per cent)	–
WD J042021.33–293426.26	TIC 179107237	×	31.09	2(2.5 per cent)	–
WD J050552.46–172243.48	TIC 169379648	×	19.34	2(11.1 per cent)	–
WD J101947.34–340221.88	TIC 71407717	×	27.54	1(17.1 per cent)	–
WD J103706.75–441236.96	TIC 146587982	×	39.10	1(36.3 per cent)	–
WD J104646.00–414638.85	TIC 106989158	×	28.23	2(13.4 per cent)	–
WD J121456.38–023402.84	TIC 349446042	×	38.04	2(0.0 per cent)	–
*WD J140115.27–391432.21	TIC 179029240	×	27.78	1(38.6 per cent)	–
WD J180345.86–752318.35	TIC 292631204	×	31.29	1(54.9 per cent)	–
WD J193538.63–325225.56	TIC 113636572	×	34.15	1(57.6 per cent)	–
WD J214810.74–562613.14	TIC 197765587	×	40.02	2(33.8 per cent)	–
WD J220552.11–665934.73	TIC 327712864	×	31.43	2(6.3 per cent)	–
WD J223607.66–014059.65	TIC 125250375	×	39.01	1(0.0 per cent)	–
WD J235419.41–814104.96	TIC 410255721	×	26.95	1(22.9 per cent)	–
*WD J090212.89–394553.32	TIC 191532802	×	36.41	1(36.8 per cent)	–
*WD J200707.98–673442.18	TIC 374346574	×	38.46	1(20.9 per cent)	–

period corresponding to the second highest peak (8.007 h) provides a poor fit to the light curve and we instead used the slightly different period (8.016 ± 0.083 h) obtained by re-analysing the full spectropolarimetry data set from Valyavin et al. (2005) supplemented with one all-night spectropolarimetry data set in the yet unpublished work of Bagnulo, Landstreet & Valyavin. The latter magnetic period provides a decent phase-folded light curve and is very close to the period corresponding to twice the period of the highest peak in the periodogram (8.017 h).

APPENDIX B: SPECULOOS OBSERVING LOG

APPENDIX C: ROTATION PERIODS OF MAGNETIC AND NON-MAGNETIC WHITE DWARFS FROM THE LITERATURE

We carefully searched the literature to compile a list of previously measured rotation periods of magnetic (Table C1) and non-magnetic (Table C2) white dwarfs. During the proofreading of the paper, we discovered a new study by Moss et al. 2023 that measured the spin period of three magnetic white dwarfs: LHS 1243, LHS 2273, and PM J15164+2803. Although they have not been included in Table C1, a preliminary test where we include the new periods indicates that their addition will not alter the conclusions drawn in this paper.

Table B1. Observational specifications for targets observed with SPECULOOS.

Name	Date (dd/mm/yyyy)	Filter	Exp. time (s)	Telescope
WD 2138-332	10-09-2021	<i>g'</i>	60	Callisto
	29-07-2022	<i>g'</i>	60	Europa
	30-07-2022	<i>g'</i>	60	Europa
	06-08-2022	<i>g'</i>	60	Ganymede
LSPM J0107+2650	16-10-2021	<i>g'</i>	1000	Europa
	17-10-2021	<i>g'</i>	1000	Europa
	29-07-2022	<i>g'</i>	1000	Europa
	30-07-2022	<i>g'</i>	1000	Europa
	06-08-2022	<i>g'</i>	1000	Ganymede

Table C1. Rotation periods taken from the literature. We ignored white dwarfs for which only an estimate or a range of possible periods was given. The listed distances were obtained from the *Gaia* catalogue (Gaia Collaboration 2021), and some temperatures and masses were taken from Gentile Fusillo et al. (2019, 2021). We assigned different abbreviations to identify the method used to measure the rotational period of a given white dwarf: Zeeman effect (Z), Polarimetry (P), Ground-based photometry (Ph), and Space-missions photometry (S). White dwarf with spin periods measured with *TESS* are marked with and asterisk.

Name	Period (h)	Spec. type	Temperature (K)	Mass (M_{\odot})	Magnetic (MG)	Distance (pc)	Detection	Ref
WD 0003-103	50.64 ± 1.08	DQ	19 420 ± 920	1.14	1.47	150.69 ± 3.22	Ph	12, 15
*WD 0009+501	8.0	DAH	6 480	0.74	0.15–0.3	10.87 ± 0.01	P	38, 39
*WD 0011-134	0.74	DAH	5 855	0.72	10	18.55 ± 0.01	P	31, 34, 49
*WD 0041-102	2.18	DBA	20 000	1.1	35	31.13 ± 0.04	Z	2, 3, 24
WD 0051+117	112.87	DAH	20 790	0.6	0.25–0.37	115.67 ± 0.73	P	44
WD 0253+508	3.79 ± 0.05	DAH	15 000	0.66	17	68.71 ± 0.18	P	1, 16, 36
WD 0316-849	0.0084	DAH	25 970	1.26	185–425	29.38 ± 0.02	Z	4, 10
WD 0553+053	0.45	DAH	5 790	0.71	20	8.12 ± 0.01	Z	3, 5, 9, 30, 41
WD 0637+477	39.16	DAH	13 980	0.75	810–1070	40.20 ± 0.04	P	44
WD 0756+437	6.68	DC	8 500	1.07	300–337	21.95 ± 0.02	Ph	8, 30, 31
*WD 0912+536	31.93	DC	7 170	0.74	100	10.27 ± 0.01	P	5, 15, 23, 49
WD 1015+014	1.75	DAH	10 000	0.91	50–90	49.39 ± 0.16	Ph	8, 13, 36, 42
WD 1031+234	3.53	DAH	15 000	0.93	500–1 000	64.36 ± 0.18	Ph	8, 35
WD 1045-091	2.75	DAH	9 819	0.81	10–70	54.12 ± 0.21	P	13
WD 1211-171	1.79	DB	12–23 000	1.15	50	90.74 ± 0.70	Ph	8, 33, 37
WD 1217+475	15.26	DAH	7 500 ± 148	0.65 ± 0.02	18.5 ± 1.0	69.54 ± 0.38	Z	45
WD 1312+098	5.42	DAH	20 000	0.86	10	101.52 ± 0.77	P	36
WD 1346+384	0.67	DAH	30 546	1.28	10	139.23 ± 1.92	Ph	20, 49
WD 1533-057	1.89	DAH	20 000	0.94	31	68.87 ± 0.20	P	1, 8, 25
WD 1639+537	1.93	DAH	7 510 ± 210	0.67 ± 0.07	13	20.14 ± 0.01	Ph	6, 14, 17, 40
WD 1743-520	68.16	DAH	20 000	1.11	36	38.92 ± 0.07	P	27, 40, 41
WD 1859+148	0.11	DAH	46 000	1.34	800	41.40 ± 0.08	Ph	11
WD 1953-011	34.6	DAH	7 920 ± 200	0.74 ± 0.03	0.1–0.5	11.57 ± 0.01	Ph	5, 7, 28
WD 2047+372	5.83	DAH	14 600	0.82	0.6	17.59 ± 0.01	P	21
WD 2051-208	1.42	DAH	21 460	1.24	0.3	31.27 ± 0.03	P	44
WD 2316+123	428.54	DAH	11 000 ± 1 000	0.86	45 ± 5	40.32 ± 0.07	Z	26, 30, 36
WD 2329+267	2.76	DAH	11 730	1.18	2.3	23.11 ± 0.02	P	15, 29
WD 2254+076	0.37	DAH	13 410 ± 130	1.30 ± 0.01	16.1	45.51 ± 0.21	Ph	43
WD 2209+113	0.02	DAH	9 021 ± 160	1.27	15	68.86 ± 1.54	Ph	19
*WD 2359-434	2.69	DA	8 390	0.83	0.1	8.33 ± 0.01	P	21
Gaia DR3 4479342339285057408	0.007	DBA	31 200	1.33	<1	75.55 ± 0.55	Ph	32
SDSS J041926.91-011333.4	1.65	DAHe	7 281.22	0.78	34.0	64.93 ± 0.45	Z	48
SDSS J073227.97+662309.9	34.3	DAHe	8 509.68	0.82	99.1	72.18 ± 0.44	Z	48
SDSS J075224.18+472422.5	1.21	DAHe	7 248.96	0.79	21.0	89.35 ± 1.24	Z	48
SDSS J075429.33+661105.7	1.37	DAHe	7 274.33	0.74	56.1	41.21 ± 0.09	Z	48
SDSS J125230.93-023417.72	0.0881	DAEH	7 856 ± 101	0.58 ± 0.03	5 ± 0.1	77.1 ± 0.7	Z	46
WD J143019.29-562358.33	1.439	DAHe	8 500 ± 170	0.83 ± 0.03	5.8–8.9	66.33 ± 0.42	Z	47
SDSS J150057.85+484002.3	1.42	DAHe	8 225.29	0.79	19.0	115.21 ± 1.77	Z	48
SDSS J152934.98+292801.9	38.15	DAH	11 920 ± 190	0.97	0.07	87.18 ± 0.60	Ph	18
SDSS J161634.37+541011.4	1.59	DAHe	7 937.51	0.75	6.5	93.69 ± 0.86	Z	49
LP 705-64	1.21	DAHe	8 440 ± 200	0.81 ± 0.04	9.4–22.2	52.66 ± 0.24	Z	47
ZTF J1901+1458	0.12	DC2	46 000	1.3	600–900	41.40 ± 0.08	Ph	11

Note. 1-Achilleos & Wickramasinghe (1989); 2-Achilleos et al. (1992); 3-Angel (1977); 4-Barstow et al. (1995); 5-Bergeron, Leggett & Ruiz (2001); 6-Brinkworth et al. (2004); 7-Brinkworth et al. (2005); 8-Brinkworth et al. (2013); 9-Bues & Pragal (1989); 10-Burleigh, Jordan & Schweizer (1999); 11-Caiazzo et al. (2021); 12-Dufour et al. (2008); 13-Euchner et al. (2005); 14-Ferrario et al. (1997); 15-Ferrario et al. (2015); 16-Friedrich, Koenig & Schweizer (1997); 17-Greenstein, Henry & Oconnell (1985); 18-Kilic et al. (2015); 19-Kilic et al. (2021); 20-Külebi et al. (2009); 21-Landstreet et al. (2017); 22-Lawrie et al. (2013a); 23-Liebert (1976); 24-Liebert et al. (1977); 25-Liebert et al. (1985); 26-Liebert et al. (1985); 27-Martin & Wickramasinghe (1978); 28-Maxted et al. (2000); 29-Moran, Marsh & Dhillon (1998); 30-Putney & Jordan (1995); 31-Putney (1997); 32-Pshirkov et al. (2020); 33-Reimers et al. (1996); 34-Bergeron, Saffer & Liebert (1992); 35-Schmidt et al. (1986); 36-Schmidt & Norsworthy (1991); 37-Schmidt et al. (2001); 38-Valyavin et al. (2005); 39-Valyavin et al. (2008); 40-Wegner (1977); 41-Wickramasinghe & Martin (1979); 42-Wickramasinghe & Cropper (1988); 43-Williams et al. (2022); 44-Landstreet & Bagnulo (private communication); 45-Gänsicke et al. (2020); 46-Reding et al. (2020); 47-Reding et al. (2023); 48-Manser et al. (2023); 49-Lawrie et al. (2013b); 50.-Angel & Landstreet (1971).

Table C2. Spin periods of non-magnetic white dwarfs measured using Kepler light curves of pulsating DA white dwarfs (Hermes et al. 2017a). The distances were obtained from the *Gaia* catalogue (Gaia Collaboration 2021).

Name	Period (h)	Spec. type	Temperature (K)	Mass (M_{\odot})	Distance (pc)	Ref
WD 0133–116	37.8	DAV	12 300	0.62	32.74 ± 0.26	1
WD 0415+271	52.8	DAV	11 470	0.56	48.25 ± 0.07	2
WD 0507+045.2	40.9	DAV	12 010	0.72	49.46 ± 0.08	3
WD 1137+423	5.9	DAV	11 940	0.71	90.47 ± 0.75	4
WD 1307+354	53.3	DAV	11 120	0.65	48.01 ± 0.07	5
WD 1349+552	41.8	DAV	12 150	0.59	69.43 ± 0.15	6
WD 1422+095	57.3	DAV	12 220	0.67	33.34 ± 0.02	1
WD 1425–811	13.0	DAV	12 070	0.69	20.89 ± 0.01	7
SDSS J1612+0830	1.9	DAV	11 810	0.78	128.63 ± 2.18	8
WD 1647+591	8.9	DAV	12 510	0.83	10.94 ± 0.02	9
WD 1935+276	14.5	DAV	12 470	0.67	18.26 ± 0.01	10
WD 0122+200	37.2	DOV	80 000	0.53	609.38 ± 29.7	11
WD 1159–034	33.6	DOV	140 000	0.54	591.36 ± 22.38	12
WD 2131+066	5.1	DOV	95 000	0.55	107.25 ± 5.23	13
KIC 8626021	44.6	DBV	30 000	0.59	377.92 ± 16.0	14
WD 0112+104	10.2	DBV	31 000	0.52	110.92 ± 0.56	15
KIC 4357037	22.0	DAV	12 650	0.62	206.31 ± 4.93	16
KIC 4552982	18.4	DAV	10 950	0.67	132.15 ± 1.36	17
KIC 7594781	26.8	DAV	11 730	0.67	172.44 ± 2.73	16
KIC 10132702	11.2	DAV	11 940	0.68	254.77 ± 10.71	16
KIC 11911480	74.7	DAV	11 580	0.58	181.88 ± 2.87	18
KIC 60017836	6.9	DAV	10 980	0.57	18.66 ± 0.01	16
EPIC 201719578	26.8	DAV	11 070	0.57	169.80 ± 4.96	16
EPIC 201730811	2.6	DAV	12 480	0.58	130.99 ± 1.32	19
EPIC 201802933	31.3	DAV	12 330	0.68	144.63 ± 2.71	16
EPIC 201806008	31.3	DAV	10 910	0.61	40.31 ± 0.06	16
EPIC 210397465	49.1	DAV	11 200	0.45	168.26 ± 3.14	16
EPIC 211596649	81.8	DAV	11 600	0.56	258.13 ± 18.32	16
EPIC 211629697	64.0	DAV	10 600	0.48	199.24 ± 7.26	16
EPIC 211914185	1.1	DAV	13 590	0.88	207.46 ± 12.82	20
EPIC 211926430	25.4	DAV	11 420	0.59	154.91 ± 2.9	16
EPIC 228682478	109.1	DAV	12 070	0.72	174.00 ± 4.66	16
EPIC 229227292	29.4	DAV	11 210	0.62	88.66 ± 0.67	16
EPIC 220204626	24.3	DAV	11 620	0.71	88.66 ± 0.67	16
EPIC 220258806	30.0	DAV	12 800	0.66	81.57 ± 0.37	16
EPIC 220347759	31.7	DAV	12 770	0.66	165.48 ± 2.91	16

Notes. 1-Giammichele et al. (2016); 2-Dolez et al. (2006); 3-Fu et al. (2013); 4-Su et al. (2014); 5-Pfeiffer et al. (1996); 6-Bognár et al. (2016); 7-Bradley (2001); 8-Castanheira et al. (2013); 9-Kepler et al. (1995); 10-Pech & Vauclair (2006); 11-Fu et al. (2007); 12-Charpinet, Fontaine & Brassard (2009); 13-Kawaler et al. (1995); 14-Østensen et al. (2011); 15-Hermes et al. (2017b); 16-Hermes et al. (2017a); 17-Bell et al. (2015); 18-Greiss et al. (2014); 19-Hermes et al. (2015); 20-Hermes et al. (2017c).

This paper has been typeset from a $\text{\TeX}/\text{\LaTeX}$ file prepared by the author.